T-2327

ELECTROMAGNETIC RADIATION FROM ROCK FAILURE

by

David R. Hanson

ProQuest LLC.
789 East Eisenhower Parkway
P.O. Box 1346
Ann Arbor, MI 48106 – 1346

T-2327

A thesis submitted to the Faculty and the Board of Trustees of the Colorado School of Mines in partial fulfillment of the requirements for the degree of Master of Science in Geophysical Engineering.

Golden, Colorado

Date April 25, 1980

Signed: David R. Hanson

David R. Hanson

Student

Approved: George V. Keller

George V. Keller

Thesis Advisor

Golden, Colorado

Date April 25, 1980

Philip R. Romig

Philip R. Romig

Head of Department

ABSTRACT

Experimental work performed in a laboratory environment has shown that the formation of failure zones within rocks is accompanied by the emission of significant amounts of radio frequency electromagnetic energy. This radiation was detected using nonresonant antennas. Rock types for which emission was observed include granite, quartzite, and taconite, while sandstone and marble did not emit measurable radiation. Amplitude spectra of the radiation showed the energy to be sharply peaked between 10 kHz and 40 kHz. It also appeared to be directional with the direction of maximum radiation colinear with that of crack growth. In addition, amplitude of RF emission increases with increasing crack size. Since emission was observed only for brittle quartz-bearing rocks, it appears the formation of piezoelectric fields is a necessary condition for RF radiation. Plausible mechanisms for emission include rapid decay of piezoelectric fields accompanying the sudden release of stress at failure and/or the acceleration of an "exoelectron plasma" through the intense local piezoelectric fields.

Since emission amplitude increases with the scale of failure, and since antennas do not need to be coupled

directly to rock surfaces as with conventional geophones, the possibility of developing an extremely portable system to monitor seismically active areas exists.

CONTENTS

ILLUSTRATIONS

ACKNOWLEDGMENTS

The author wishes to express his gratitude to Professor George V. Keller of the Colorado School of Mines for acting as advisor on this project and to Professors Maurice W. Major and Fun-Den Wang, also of the Colorado School of Mines, and Dr. Glen A. Rowell of the United States Bureau of Mines for serving as members of my committee.

My special thanks to Dr. Glen A. Rowell, Dr. Brian T. Brady, and Dr. Maurice W. Major for their long hours of advice and consultations throughout this project. Thanks also to Norm Stenerson of the USBM for his aid in laboratory work, and to Robert G. Shaw, James C. Bean, and Dianne Smith, also of the USBM, for their invaluable assistance in photography, drafting and typing.

The equipment used in this work was provided by the United States Bureau of Mines and would not have been available but for the support of Verne E. Hooker. Financial assistance was supplied by the United States Bureau of Mines and a research assistantship from the Colorado School of Mines and is hereby gratefully acknowledged.

I. Introduction

The search for precursory phenomena and a reliable method for failure prediction and stability monitoring of rock materials has been extensively pursued since Griffith's 1920 and 1924 works in the Transactions of the Royal Philosophical Society of London on the theory of rupture. Unfortunately, despite the volumes of work produced, there has yet to be found a workable method of failure prediction which is generally accepted. Hence the search for a better understanding of rock failure on both a microscopic and macroscopic scale continues.

The failure of crystalline lattice material is a complex process whose exact mechanism is not well understood. For this reason, many conflicting theories of failure have been advanced, each with its own strengths and weaknesses. These include Griffith, Navier (1), diffusion, dilatancy, (2,3,4,5,6,7), and inclusion theories, (8,9,10,11). Because of this obvious disagreement on the mechanism of failure, a reliable method of failure prediction has not been found. Hence any information which might shed light on the mechanism of failure is of value.

The purpose of this work is to investigate the emission of radio frequency (RF) electromagnetic (EM) energy

upon the formation of failure zones in rocks. These emissions are studied with a view toward both a better understanding of failure processes and development of a possible failure monitoring system.

A series of samples of granite, quartzite, taconite, sandstone, and marble were tested for EM radiation as they failed under uniaxial compression. In addition to an array of three antennas to pick up RF energy, load, two orthogonal moments, acceleration, and acoustic emission were monitored. These data are interpreted and possible mechanisms reviewed.

II. Previous Work

The observation of bursts of high frequency electromagnetic radiation accompanying the deformation and failure of rocks is a fairly recent development and published data is limited. In her book, Parkhomenko (12) mentions that fragmentation of LiF and NaCl crystals gives rise to EM radiation and visual luminescence, with the amplitude of light and nonvisible EM radiation nearly proportional to each other. However, no quantitative results were presented. Vorobev, et al. (13) scratched various dielectric materials with a diamond pyramid and observed pulsed radio frequency emission. This work was performed on glass and single crystals of LiF, KCl, NaCl, quartz, feldspar, flourite, and talc. For soft materials and low scratch loads no radiation was observed. For harder materials the intensity of radiation was found to increase to a saturation level as load on the indentor and hardness of the material increased.

Some of the first work with rock aggregates was performed by Nitzan (14). He observed the emission of exponentially decaying bursts of EM radiation in the frequency range of 1 MHz to 10 MHz accompanying the fracture of hard piezoelectric materials. Nitzan's detection apparatus consisted of a ferrite-core AM radio coil and amplifier.

Samples were stressed in uniaxial compression, by pressing a steel ball against a flat surface, and by crushing irregular samples in a vise. For all quartz-bearing materials tested (granite, granodiorite, sandstone, and quartzite) RF signals were detected, while for nonpiezoelectric samples (basalt, obsidian, limestone, aluminum, steel, glass, and plastic) no signals were observed.

From this evidence Nitzan proposed that the most probable mechanism of emission was the rapid decay of the piezoelectric field which resulted from the sudden stress release as the sample cracked. Frequency content of the signal would be related to the rate of stress release and hence to the grain size of the material. This relationship was observed by Nitzan as the spectra of bursts shifted to higher frequencies as grain size decreased. Nitzan also suggested that emission should extend into higher frequencies than the 10 MHz upper limit in his work.

Experimental and theoretical work was performed during the 1960's and 1970's on the generation of transient EM radiation by elastic pulses in metals (15,16,17). The metals are considered to be composed of a fixed positively charged lattice of atoms permeated with a negatively charged free electron gas. As an elastic pulse is propagated along the lattice the differential motion between

the electron gas and lattice gives rise to the EM radiation as predicted by Maxwell's equations. Although this work has been done exclusively with highly conductive metals, the application of this mechanism to rock materials may be appropriate. That is, the rapid movement of a dielectric rock through electric and magnetic fields as the substance fails may contribute to observed emission.

Finally, in his review paper on earthquake lights, Derr (18) has reported that sferics in the 10 kHz to 20 kHz range have accompanied earthquakes and luminescence. In addition, Derr reported the occurrence of strong noise over the entire FM broadcast band as received on an automobile radio after the July 16, 1973, earthquake in Guerrero State, Mexico. This radio noise reportedly lasted five minutes. The two mechanisms advanced by Derr for both luminescence and RF radiation were 1) violent low-level air oscillations, and 2) excitation of the piezoelectric effect in quartz-bearing rocks. Although Derr did not specifically deal with RF electromagnetic radiation, he did attempt to present evidence that significant amounts of electromagnetic radiation has been reported to accompany large-scale failure in earthquakes.

III. Experimental Procedure

NX size (55 mm diameter) cores of Red Texas Granite, Barre Granite, Pikes Peak Granite, Dakota Sandstone, Carthage Marble, and a quartzite from the Galena Mine, Wallace, Idaho, were cut and ground to a final length of 13.5 cm for use in uniaxial compression tests. In addition, a number of smaller samples of Mather Iron Ore from the Marquette District of Michigan were prepared. A complete listing of sample sizes is included in Appendix A. All samples were tested to failure in uniaxial compression in a servo-controlled materials testing system (MTS Systems Corporation, 2.7×10^6 N capacity). Displacement rates for all tests was held at 5×10^{-6} m/sec. (Reference to specific trade names is made for identification only and does not imply endorsement by either the Colorado School of Mines or the United States Bureau of Mines.)

Two load cells were used to instrument the tests. Both allowed monitoring of load (F_z), and two orthogonal moments (M_x and M_y). The first load cell (Interface model 1240 HF, 9×10^5 N and 16×10^3 N-m capacity) allows detection of load changes greater than 90 N. However, the noise level of monitoring devices used reduces this resolution to about 500 N. Maximum thrust and moment deflection are 1×10^{-4} m and 0° 15' respectively. The cell has an

approximate Q value of 10 and resonant frequencies of 800 Hz, 1100 Hz, and 3300 Hz. The other load cell monitors the same load and moments through an array of strain gauges mounted on a steel cylinder. Resolution of load changes with this cell is nearly identical to the Interface load cell although there is slightly more noise. Resonant frequencies exist at 20 kHz for the vertical load and 10 kHz to 15 kHz for the moments. Only the output of the second load cell was recorded on magnetic tape during tests. Although it was slightly noisier, this cell exhibited less ringing due to its higher resonant frequencies.

A single piezoelectric polymer transducer (PPT) was placed directly on the sample surface and was held in place by an elastic rubber sleeve placed over the entire sample. Coupling between the PPT and rock was provided by an ultrasonic couplant (Ultragel II, Ultrasonic Couplant, Echo Laboratories). The PPT was supplied by the National Bureau of Standards (19,20). The transducers are produced by evaporating a film of aluminum on both sides of a polymer film, often polyvinylchloride or polyvinylfluoride. The film is made piezoelectric by heating and then cooling it in the presence of an electric field. Voltages are induced across the leads of the transducer by elastic deformation of the film as with conventional piezoelectric devices. The PPT

responds primarily to pressure waves of elastic displacements originating within the sample, but will also respond to changes in temperature and strain. Advantages of the PPT include its short ring-down time (several microseconds) which allows the identification of closely spaced impulsive events, the PPT's ability to conform to the shape of the rock, and its small mass (.3 gram). The PPT output was input to a 20 db gain amplifier before being recorded. In all tests the PPT was positioned along the +X axis of the sample.

An Endevco model 2219E accelerometer and a Dunegan/Endevco model D9201 acoustic emission transducer (AET) were coupled to the base plate of the press to monitor acoustic signals transmitted through the specimen and press. Both were coupled to the press by means of a coupling gel (Sperry Multipurpose Ultrasonic Couplant, heavy viscosity, #50A4084). The AET has an optimum operating frequency range of 100 kHz to 1 MHz with a maximum response of .1 mv/microbar at 200 kHz. The accelerometer has a peak response of 380 mv/g with a 100 pf load. Its response is essentially flat from 100 Hz to 4 kHz with a resonant peak at 16 kHz. Output from both the AET and accelerometer were directed through a 20 db gain amplifier before being recorded.

The electromagnetic radiation detection devices consisted of three electrically short dipole antennas. These were constructed from a piece of 18 gauge insulated wire soldered to the center conductor of an open BNC connector. Length of each dipole was 15.25 cm, corresponding to a quarter wavelength of a 1967 MHz electromagnetic wave. The radio frequency signals emitted from the sample and detected with the dipole antennas were input to a 40 db gain preamplifier (DC - 200 kHz, down 12 db at 1 MHz). The signal was then band pass filtered from 10 kHz to 400 kHz to remove lower frequency environmental noise encountered in the laboratory. Finally, another 20 db of gain was applied before inputting the signal to one channel of the tape deck. The three antennas were arrayed at 120° intervals approximately 12 cm from the sample in an attempt to obtain information on the location of cracks (Figure 3).

Data from all these monitoring devices were recorded on an analog Sangamo/Schlumberger Sabre X magnetic tape deck. In the FM recording mode, a frequency range of DC to 160 kHz may be recorded at 240 ips. For these tests all recording was done in the FM mode due to its superior signal to noise ratio over direct analog recording. Recording speed in all tests was 240 ips. This speed was used to obtain the highest possible frequency range available

Figure 1: Laboratory setup used in experimentation performed at the United States Bureau of Mines, Denver Research Center.

Figure 2: Typical instrumentation of rock samples showing position and orientation of PPT and antenna.

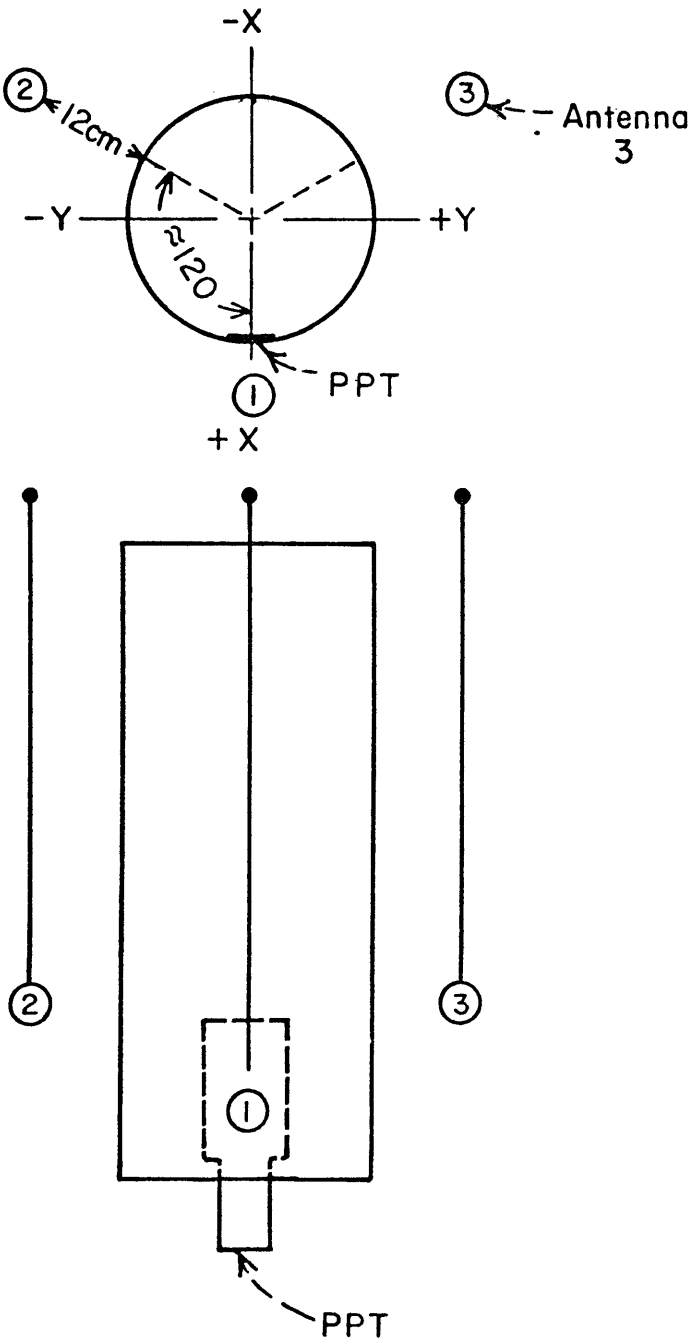

Figure 3: Schematic of rock sample showing the location and orientation of antennas and PPT. Letters +X, -X, +Y, -Y refer to orientation and directions of X and Y axes for moments.

in the FM mode. Data may be recorded in one of two sensitivity ranges, the first allowing a signal of between 1 and 10 VRMS and the second a signal between .1 and 1 VRMS. Output from each of the three antennas was recorded on two channels, one at the 1-10 VRMS scale, and the other at the .1-1 VRMS setting. All other data channels were recorded using the 1-10 VRMS scale setting.

When working with multiple data tracks it is desirable to know the absolute time differences between events on different channels. Unfortunately, the time differences observed upon playback of the data are not only a function of the different occurrence times of the events, but also a function of the misalignment between recording and playback heads. That is, if one signal is input simultaneously to two channels, when played back there should be no phase shift observable between the two if the heads are in perfect alignment. This is unrealistic as there is inevitably skew present between record and playback heads. A value for this skew was obtained as follows: A band-limited (DC to 100 kHz) "white" noise signal was recorded simultaneously on all 14 tracks available on the Sabre X at a tape speed of 120 ips in the direct recording mode. Pairs of channels were then played back at 60 ips and input to a Fourier analyzer which computed and displayed the phase

differences between the two. Because the tape was played back at one-half the recording speed, frequencies observed from the tape playback were halved and the phase and time shifts doubled. Phase shifts were measured at a frequency of 50 kHz and time shifts computed by:

$$T = (1/f)\ (\phi/360)\ (10^6\ \mu sec/sec)$$

$f = 50000$ Hz

ϕ = observed phase shift in degrees

T = time shift between channels in microseconds

The phase differences and time shifts computed at 60 ips are shown in Appendix B. From these measurements time differences due to head misalignment between any two of the 14 channels may be computed. Actual time shifts present at a recording speed of 240 ips will be one-fourth those shown for a speed of 60 ips in Appendix B. The relation between phase and frequency observed with the Fourier analyzer was very nearly linear for all channel pairs. Because of this linearity the time shift computed at 50 kHz is the same for all frequencies.

In addition to time delays due to head misalignment, shifts are present between antenna signals and all other data. This is due to the different speed of propagation of the signal (acoustic vs. speed of light). Appendix B deals with the method employed to attempt to remove this shift and bring all data into time coincidence.

In addition to the Sabre X tape deck, output from the load cell, PPT, AET, and antennas was monitored on four digital memory oscilloscopes (Nicolet Corporation, models 1090A and 2090). Each digital scope has a sampling rate that can be varied from .5 microsecond to 200 second per point. Each sweep consists of 4096, 12 bit points. Records from the 1090A oscilloscopes were recorded on a Kennedy model 9700 tape deck after processing through a Nicolet model 283A interface. Records from the model 2090 oscilloscope were recorded on its own magnetic disk. By using the Nicolet scopes, parallel output between the Sabre X and Kennedy tape decks was obtained, ensuring data acquisition should one system malfunction.

The equipment configuration and experimental procedure as described above is the "final" system used in these experiments. That is, the information monitored and frequencies used seemed to give the best results. This configuration was not, however, arrived at without considerable experimentation. It is felt that a description of these trials and the conclusions drawn from them is warranted to help substantiate the final experimental design. The PPT, AET, accelerometer, and load cells had already shown their usefulness and practicality in previous tests (21). Their design has been shown to be workable in previous experi-

ments performed at the USBM.

The original aim of the new set of experiments was to incorporate the detection of EM radiation with the monitoring of all other data. This neccesitated designing an antenna system capable of detecting the frequencies expected from rocks bursts. Previous work by Nitzan (14) had shown the the frequency content of RF signals from the fracture of quartz and tourmaline crystals and samples of sandstone and granite to extend from 1 MHz to 10 MHz. It was felt that emission should also exist at much higher frequencies; so, to search in these higher frequencies, a "bow-tie" antenna was constructed which had a length equal to a quarter wavelength of a 347 MHz electromagnetic wave (22,23,24,25). The "bow-tie" configuration was chosen because of simplicity, ease of construction, and broadband characteristics. This antenna exhibited fairly good response between 175 MHz and 347 MHz, although resonant peaks existed in its response curve. The antenna output was fed successively through a 200 to 50 ohm transformer, a 50 ohm Tektronix Type 011-0049-01 line terminator, to a 41.3 db gain Watkins-Johnson amplifier (41.3 db, 5 MHz-1000 MHz). The amplified signal was then viewed on a Tektronix Type 7623 oscilloscope with a Type 7B92 Time Base capable of a setting of .5 nanoseconds per cm. After amplification the ambient noise level in the

lab was much larger than expected with an average amplitude of 1.5 to 2.0 volts peak-to-peak and transient bursts up to 6 volts peak-to-peak. The very high amplitude transients were traced to switching of nearby electrical equipment. These transients were picked up by the antenna despite having all power supplied through a voltage regulator to eliminate bursts or sudden drops in line voltage. Using the bow-tie system described above, several tests were performed on granite samples with no EM radiation observable above the noise level.

A number of schemes were proposed to reduce the ambient noise. The first of these was to wrap the entire testing machine with an aluminum foil electrostatic shield. This had no observable effect on the noise. Still believing adequate shielding was all that was needed for experimental success, a Soiltest press (175000 lbs. capacity) along with the antenna system was moved to the electrostatically shielded room of the Physics department of the Colorado School of Mines. This room is grounded to the building framework and has AC power supplied to it through a series of isolation transformers to eliminate line voltage flucuations. With the door tightly closed, the ambient noise was reduced about 50 times, to an average of 20 mv peak-to-peak. Another series of tests were performed, again with negative

results. As a final attempt to reduce the ambient noise the antenna system was taken underground in the Colorado School of Mines experimental mine in Idaho Springs, Colorado. It was hoped the surrounding rock would act as a more efficient shield against unwanted RF signals. Although the amplitude of the observed noise decreased as the system was taken further into the mine, noise reduction was little better than that achieved in the shielded room.

Finally, the frequency band of investigation was lowered and narrowed from 5 MHz - 400 MHz to 10 kHz - 400 kHz. This overcame a number of problems in equipment availability. Also, other antenna were tested, including ferrite- and air-core coils and dipoles. A 15 cm dipole gave the best results.

The noise problems encountered in early work were probably due to a number of related factors. First, the inherent noise level of the amplifier, scope, and transmission line over the very broad band they were designed for is very much larger than the signal expected from the rock failure. What was originally thought to be ambient noise external to the system is now believed to be at least partially internal noise which no amount of shielding would eliminate. If, however, the frequency band could be severely limited by the use of electronic band pass filters, the

noise could probably be reduced substantially. Unfortunately, filters in the frequency range of 5 MHz to 400 MHz were not available at the USBM. Secondly, the original bow-tie antenna and subsequent coils were designed for a resonant frequency very close to the range of frequencies desired. This was done in the hope of more effectively coupling the receiving antenna to the transmitting source to get maximum power transfer. However, any noise present in the frequency band of interest would set the antenna into resonance compounding the noise problem. The best antenna, therefore, for use in this type of experiment would seem to be one whose resonant frequency is far above the frequencies of interest. This means an electrically short antenna. This design criteria is analagous to that of geophones whose operating frequencies are set far below their resonance. Besides these "internal" noise sources, external sources such as switching transients, AC line noise, and ambient environmental noise compounded problems in the high frequency range. Finally, while no emission was observed in the 5 MHz to 400 MHz range due at least partially to noise, it is felt that emission probably does exist at these frequencies and may be observable with the proper antenna and narrow band filters.

IV. Results

A. Galena Quartzite: Test # 47

Galena Quartzite is a fine-grained, light gray quartzite occasionally banded with veins of quartz, pyrite, galena, siderite, silver, and tetrahedrite. It is the country rock from the Galena Mine, Wallace, Idaho. Samples were prepared from cores obtained from the drilling of holes for geophone mountings on the 4000 foot level of the mine. Care was taken to select samples for testing which were free from obvious fractures and veining.

Devices used to monitor the tests on Galena Quartzite were an accelerometer, AET, axial load, two orthogonal moments, and three antennas. Due to the high strength and violent nature of the failure of this rock, no PPT's were used for fear of destroying the limited number of these devices available. The event examined here for Galena Quartzite is one of a number of preliminary fractures and is associated with a load drop of 47 kN. Figures 4 through 15 are the results from this preliminary fracture. The final failure of the sample involved a load drop of over 400 kN.

Fracture of the sample is assumed to coincide with the rapid load drop from 538 kN seen on Figure 4 at 0.90 msec. This rapid load drop corresponds quite well with the onset of violent changes in both components of moment (Figures 5

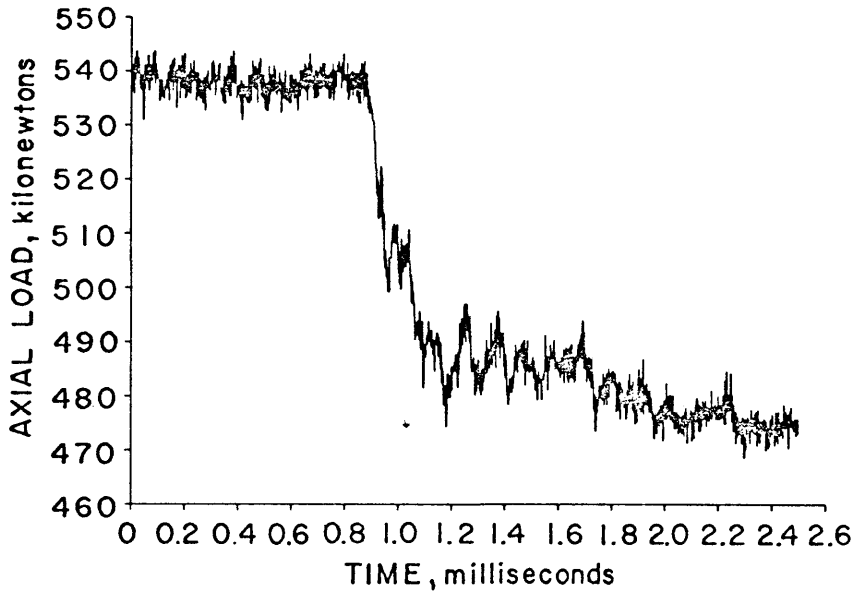

Figure 4: Axial load for a preliminary failure of Galena Quartzite #47. Load drop began at 0.90 msec and totaled approximately 47 kN.

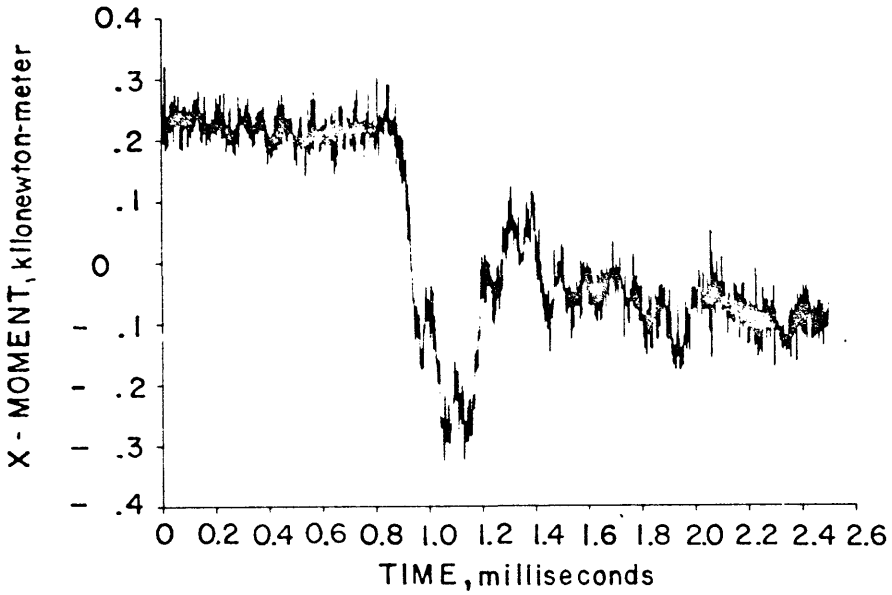

Figure 5: X component of moment for Galena Quartzite #47. Decreasing moment indicates movement of load-bearing axis toward the -Y direction and vice versa. The rapid decrease in moment at 0.89 msec. corresponds to the inception of failure in figure 4.

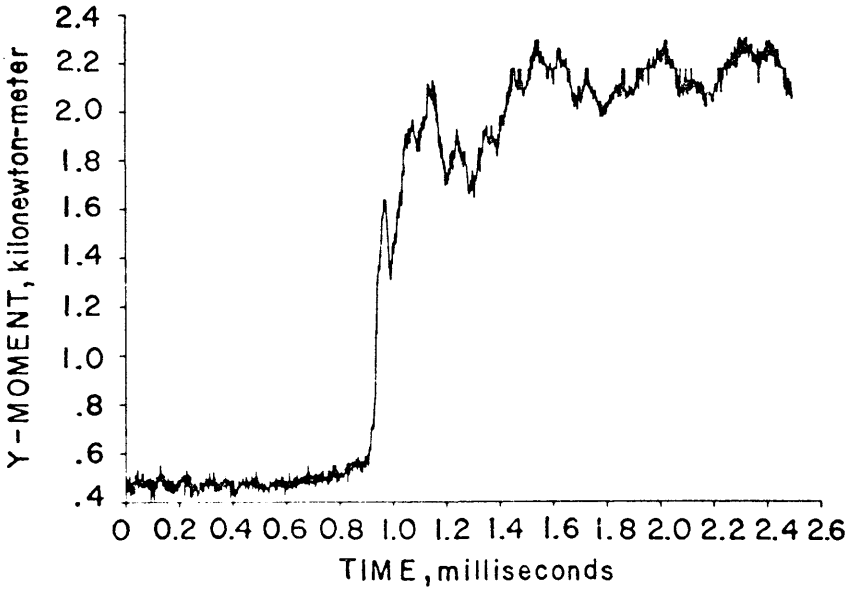

Figure 6: Y component of moment for a preliminary fracture of Galena Quartzite #47. Increasing moment indicates movement of the load-bearing axis toward the -X direction and vice versa.

and 6). Moment changes can be interpreted as shifts of the load-bearing axis toward more competent rock as the sample fails. This, in turn, can be used to interpret the direction of growth of a fracture. Since a left-handed coordinate system was used, an increase in the X moment indicates a shift of load toward the +Y axis, and an increase in Y moment corresponds to a shift of load-bearing axis toward the -X axis. The orientation of axes and antennas is shown in Figure 3. The magnitude of the changes in M_y in Figure 6 are much larger than those in M_x indicating most of the sample's tilt occured about the Y axis. From these moments it can be inferred that the crack grew from the +X to -X direction, or vice versa. It should also be noted that the recovery of load at 0.97 msec on Figure 4 corresponds to a sudden moment reversal or shift of the load-bearing axis back toward the center of the sample. This type of behavior was seen in all tests and may be interpreted as the recovery of dilatancy and closure of cracks as the steel platens advance on the sample. This will momentarily increase the competency of the rock as the cracks close and friction takes effect. The violent, rapid variations in moment reflect the extreme instability of the sample both before and during failure. Before fracture, the loading axis is nearly in the center of the sample (zero moments). As the sample fails it

violently shifts its load-bearing axis in the direction of more competent rock, with some reversals. This load shift puts more and more stress on a smaller area along with increasing tilt on the region of already fractured rock which accelerates the eventual failure of the sample along these axes.

The accelerometer (Figure 7) became overdriven early in the test and continued ringing throughout the time window of this event.

The AET (Figures 8 and 9) begins responding at around 0.56 msec., long before any other device with the possible exception of the accelerometer. Prior to this time, output of the AET is quite low and it is possible that the 20 db amplifier for the AET became overdriven earlier in the test and did not recover until 0.56 msec. The major response of the AET seems to begin somewhere near 0.90 msec. and so correlates with load and moments.

All three antennas arrayed around the sample showed bursts of electromagnetic energy arriving at between 0.90 and 0.92 msec. (Figures 10, 12, 14). These times are slightly late compared to other indicators of failure, but this is probably due to the uncertainty of the location of failure events. That is, this fracture may have been closer to the load cell than the 6.4 cm. assumed to compute

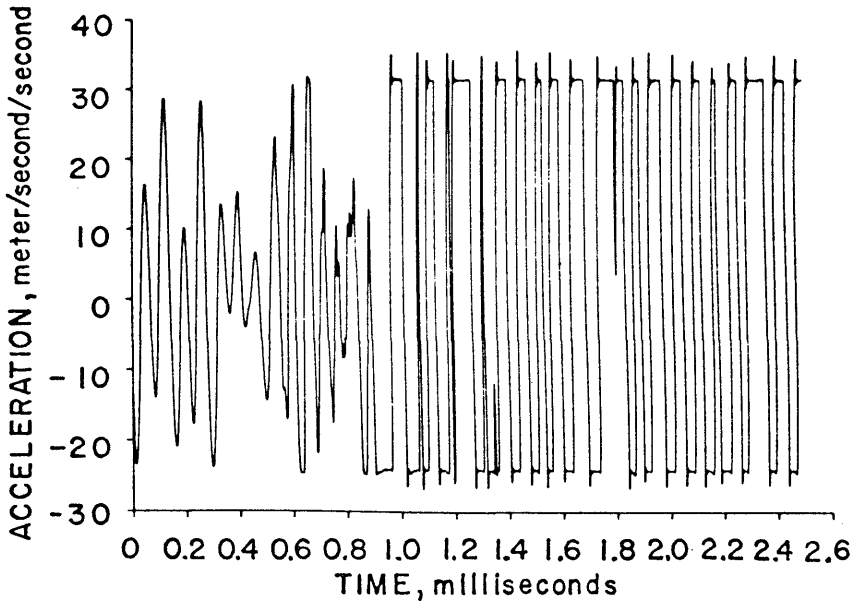

Figure 7: Accelerometer response of the same event as described in Figures 4 through 6. The accelerometer is overdriven and clipped from events which paralyzed its amplifier.

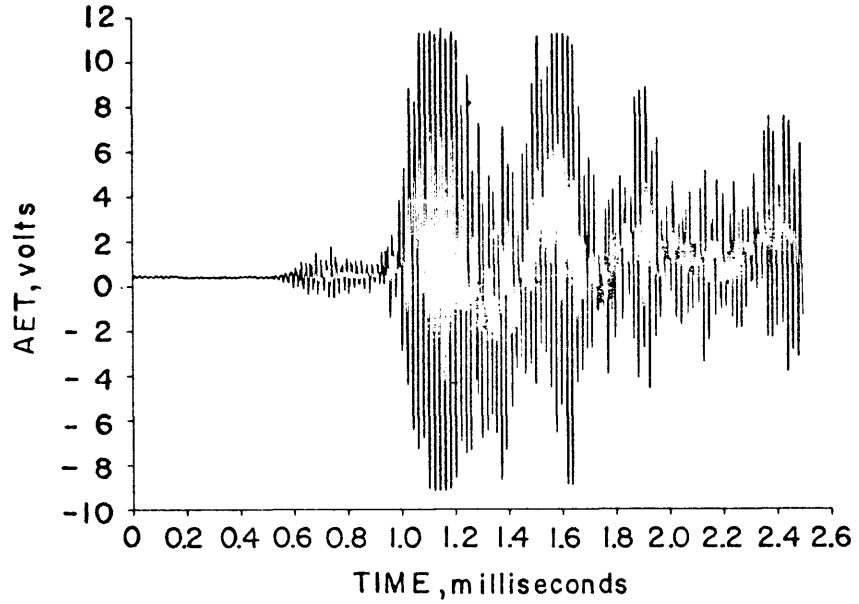

Figure 8: Output of the acoustic emission transducer for a preliminary failure in Galena Quartzite sample #47. Response begins at .56 msec. with the high amplitude signal beginning at about .95 msec.

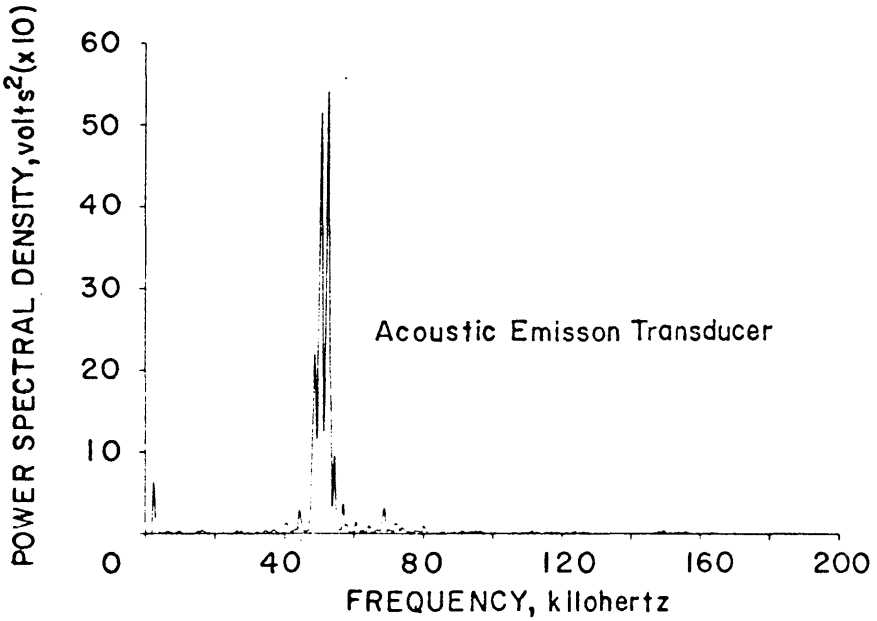

Figure 9: Amplitude spectra of AET output of Figure 7. Spectra peaks occur at 49, 51, and 53 kHz.

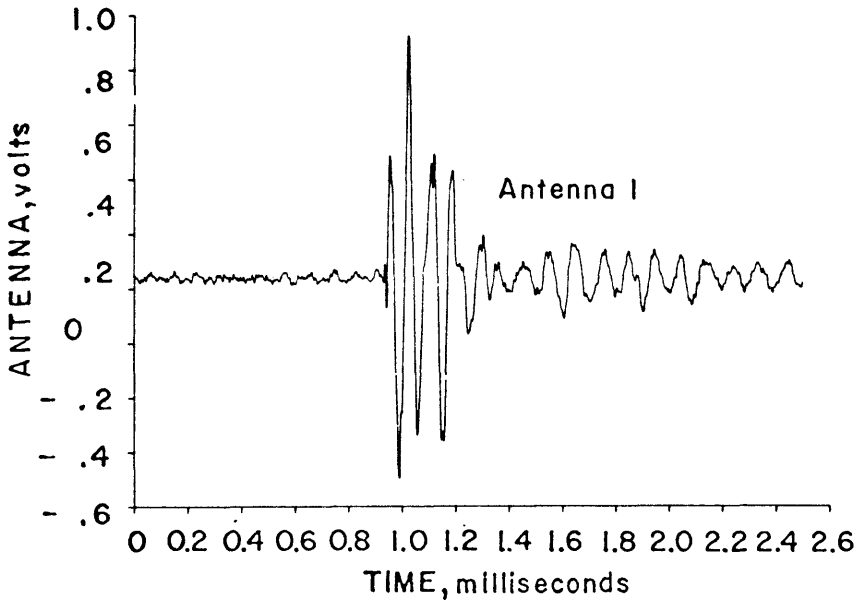

Figure 10: Response of antenna to a minor crack in Galena Quartzite #47. Signal begins at approximately 0.9 msec. and obtains a maximum peak-to-peak amplitude of 1.6 V.

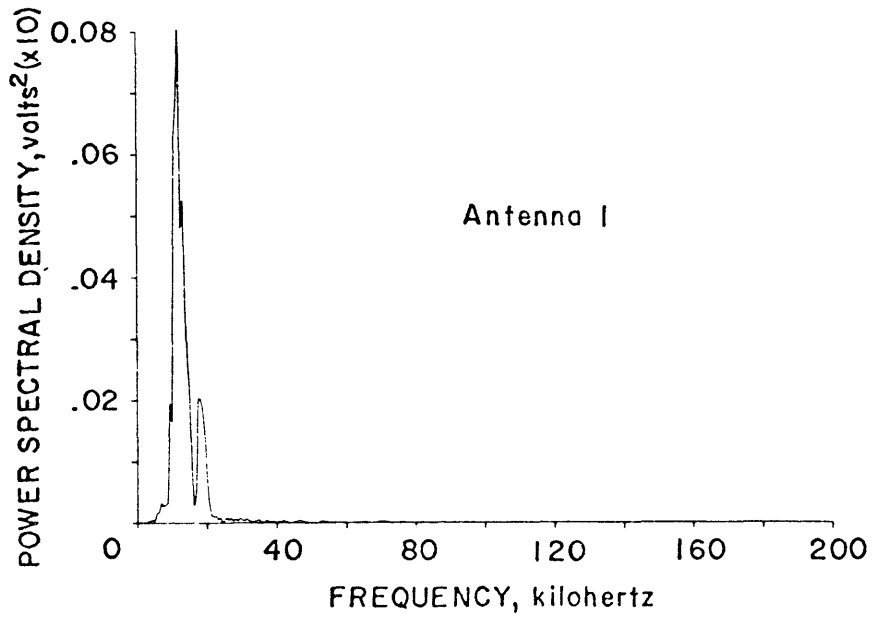

Figure 11: Amplitude spactra of the antenna signal of Figure 10 showing the very sharply peaked spectra at 12 kHz.

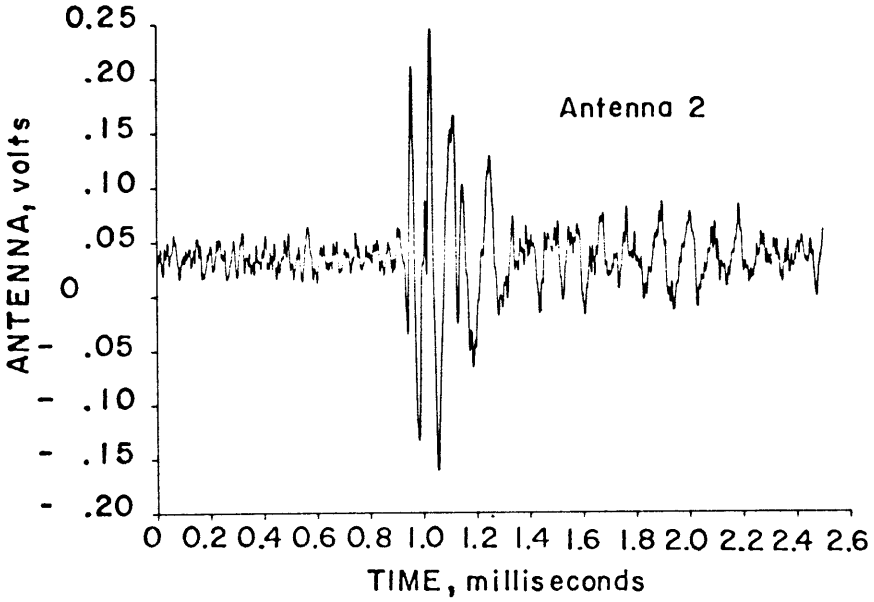

Figure 12: Antenna 2 response, still from Galena Quartzite #47. Response begins at about 0.9 msec. but has only .4 V peak-to-peak amplitude.

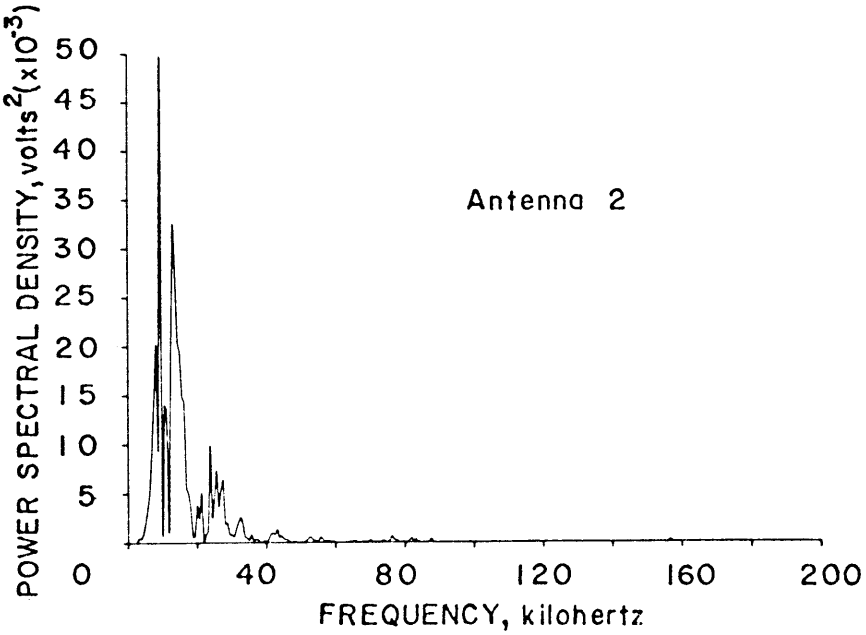

Figure 13: Spectra of antenna 2. Spectral peaks occur at 8, 9.5, and 13 kHz.

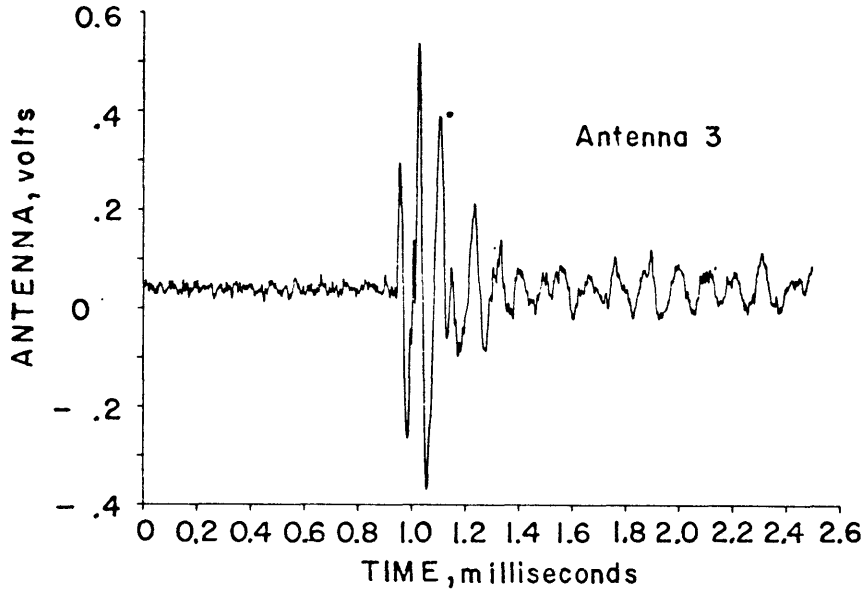

Figure 14: Response of antenna 3 to Galena Quartzite #47. Signal arrives at about .95 msec. and has a maximum peak-to-peak amplitude of .9V.

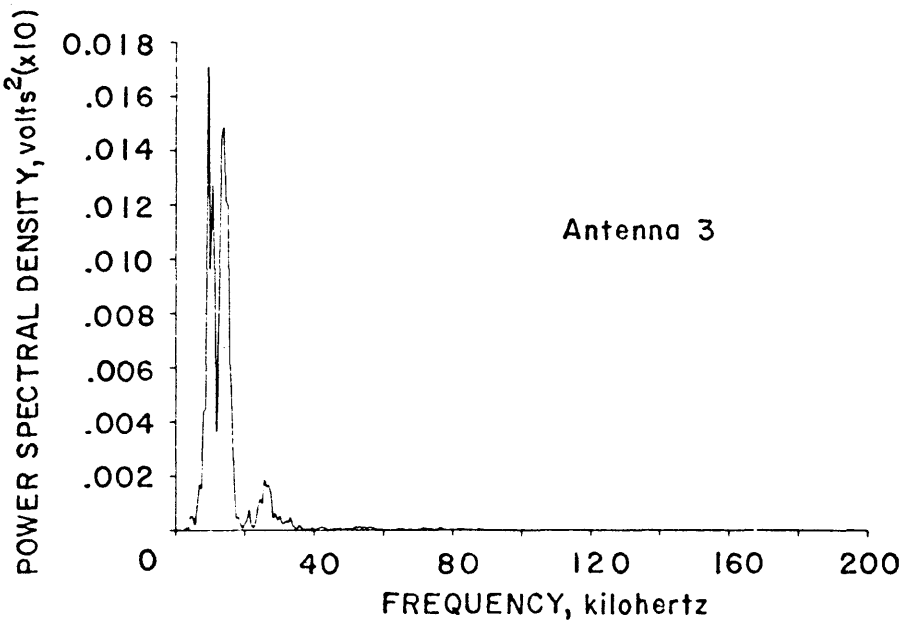

Figure 15: Spectra of antenna 3. As with antennas 1 and 2, emission is sharply peaked below 20 kHz with peaks at 9, 10.5, and 14 kHz.

average time shifts (Appendix B). This could add as much as 12 μsec to load and moment times. Also, if the velocity of acoustic signals through the failing quartzite differed from the 5334 m/sec used, additional unknown time shifts could be introduced.

The important point to note, however, is the production of a burst of radio frequency electromagnetic radiation within 50 μsec of the formation of a failure zone within the rock. This failure zone need not be associated with the final failure of the sample.

The amplifier, filter, and recording system used had a rated bandwidth of 10 kHz to 160 kHz, but spectra of antenna signals (Figures 11, 13, 15) peaked sharply below 40 kHz. This is generally the case for all tests, grain sizes, and rock types as will be shown in subsequent tests. That emission should be so sharply peaked was unexpected.

Also unexpected was the difference in amplitude (peak-to-peak) of the responses of the three antennas. Antenna 1 has a maximum peak-to-peak amplitude of 1.6 V, antenna 2, 0.4 V, and antenna 3, 0.9 V after 60 db amplification and 10 kHz to 400 kHz filtering. Two explanations for these differences present themselves. The first is that the crack was closest to antenna 1, and the farther the antenna from the crack, the lower the antenna response. The maximum difference in travel

path between antenna 1 and 2 is about 5 cm. That this distance would cause a four-fold decrease in amplitude seems unlikely unless perhaps the signal is severely attenuated by having to travel through the rock. A more plausible explanation would be that emission is directional. If, as indicated by the moments, the failure zone progressed from +Y to -Y and from +X to -X, the maximum emission might be expected to be produced colinearly with crack propagation. This is roughly what is seen in antennas 1 and 3.

Results of this test show the production of a burst of EM radiation accompanying the formation of a failure zone within the rock. In addition, the frequency content of these signals is concentrated below 40 kHz. Finally, the different amplitudes of the three antenna responses indicates a degree of directionality.

B. Red Texas Granite: Test #38

Red Texas Granite is a pink, biotite, fluorite granite. It is a coarse-grained, hypidiomorphic granular rock. Hoenig (26) submitted this rock to analysis and found its constituents to be microcline, 30%, quartz, 30%, plagioclase, 20%, biotite, 20%, and interstitial fluorite, <1%. There were traces of magnetite, apatite, and zircon, and overall alteration was considered moderate.

Because of the large grain size of Red Texas Granite,

failure of the rock in the uniaxial mode consists of a large number of preliminary cracks which gradually reduce the competency of the rock until final failure occurs. This behavior prevents the ultimate failure of the rock from being as violent or having as large a load drop as with finer grained materials. Figures 16 through 28 are the results from one of the preliminary fractures which occurred a relatively long time before catastrophic failure. No indication of any sort of event is detectable above the noise level on the load or either moment (Figures 17 and 18). Load is nearly constant at 362 kN and M_x and M_y are constant at 0.22 and 0.17 kN-m respectively. The noise on these figures is due to analog tape noise. Both the AET and accelerometer (Figures 19 and 21) begin responding at about 1.0 msec and continue ringing throughout the remainder of the trace.

Again all three antennas (Figures 23 to 28) show a very sharp, short duration burst of electromagnetic energy commencing at about 0.96 msec. This response time is earlier than the AET and accelerometer response, but this again may be due to uncertainty of the location of the event within the sample. The important points of the antenna responses are their short duration (about 100 μsec), differing amplitudes, and sharply peaked spectra. If the antennas were excited by the voltages created by the AET or accelerometer,

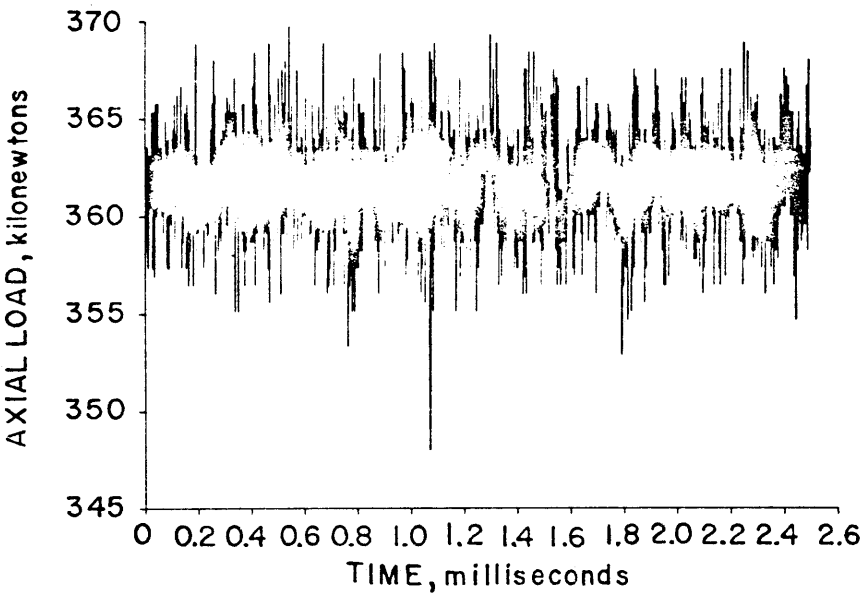

Figure 16: Axial load of a preliminary failure of Red Texas Granite sample #38. Note the constant load of 362 kN with no indication of a load drop. Fuzz on the trace is due to analog tape noise.

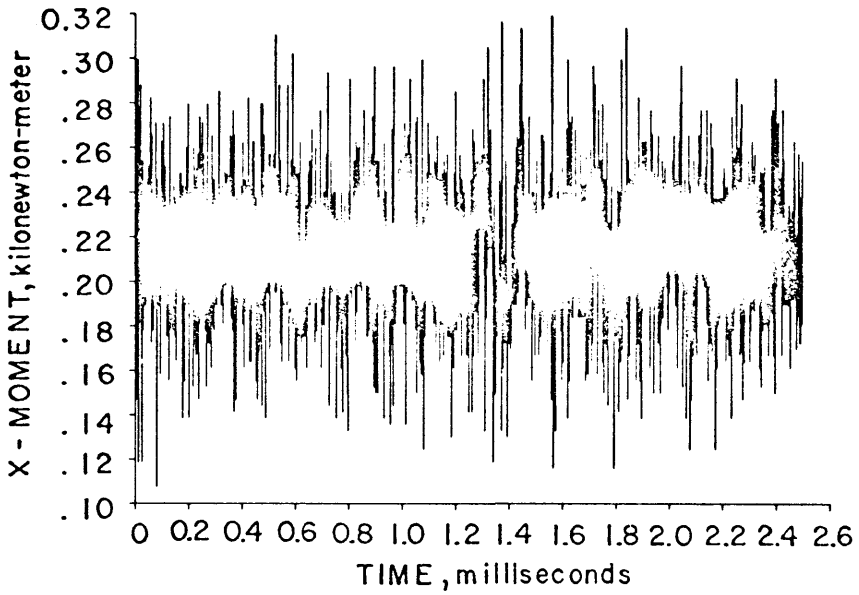

Figure 17: X component of moment for Red Texas Granite #38. There is no indication of any changes indicative of failure.

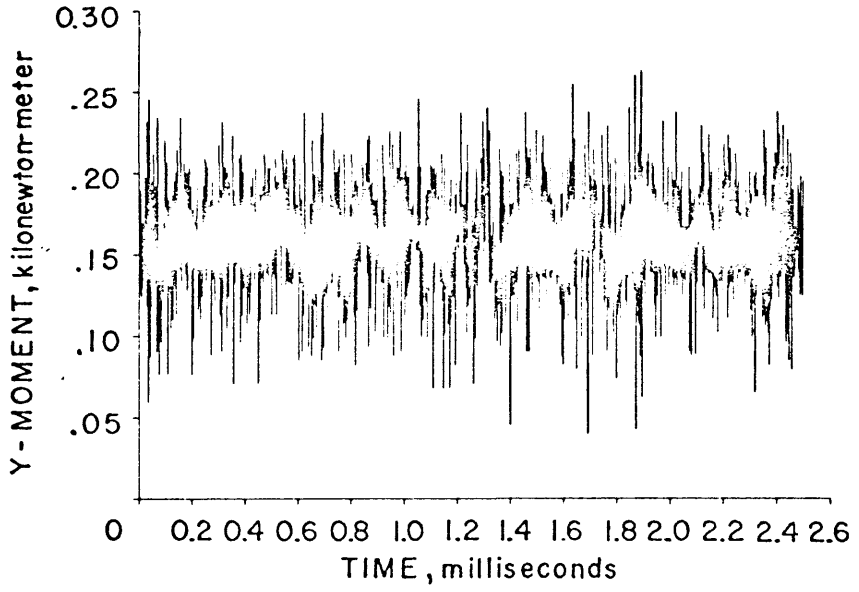

Figure 18: Y component of moment, Red Texas Granite #33. Again there is no change from the constant value of .17 kN-m other than analog tape noise.

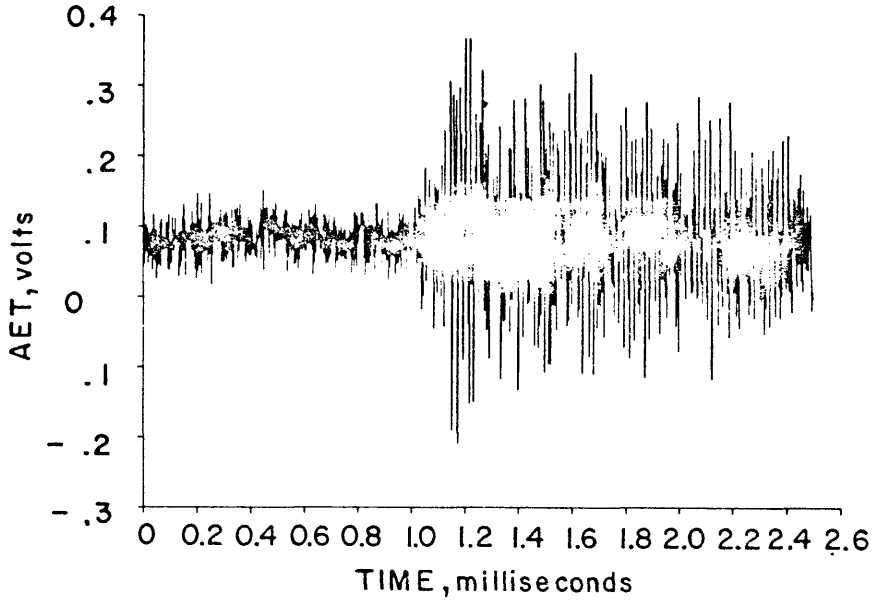

Figure 19: Acoustic emission transducer output with preliminary fracture of Red Texas Granite sample #38. AET response begins at approximately 1.0 msec.

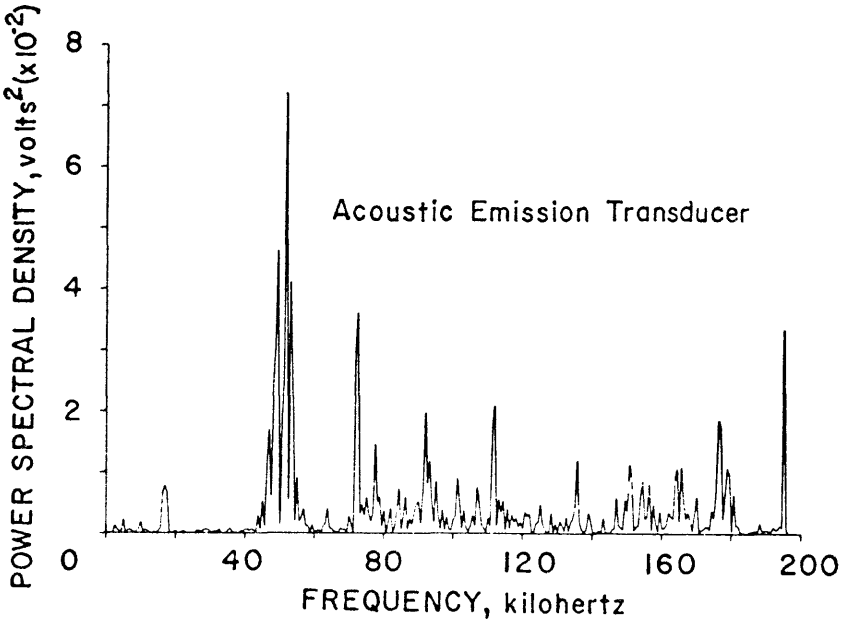

Figure 20: Power spectra of Figure 19, AET. Spectrum has peaks at 50,52, 53 and 75 kHz. The spread of energy is indicative of the noisier trace of Figure 19.

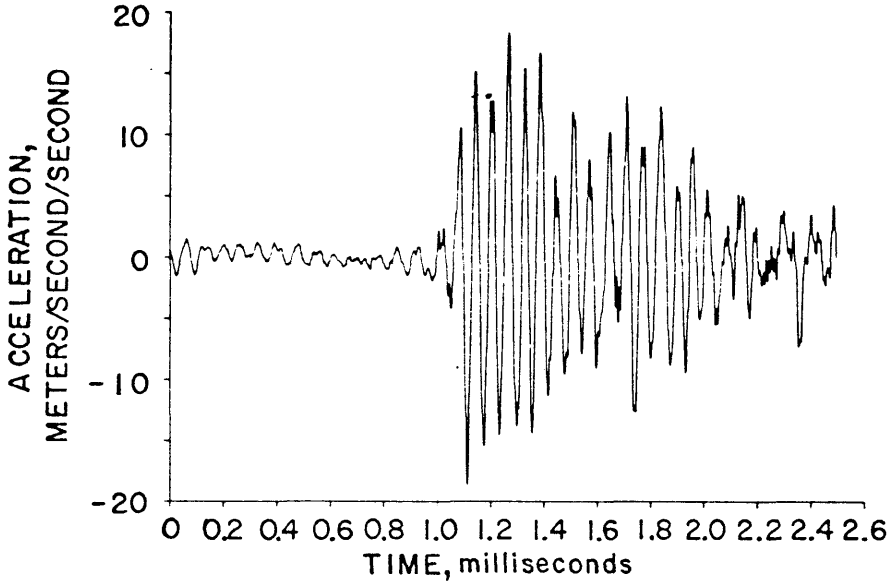

Figure 21: Acceleration of the base plate of the rock press resulting from the preliminary fracture of sample #33.

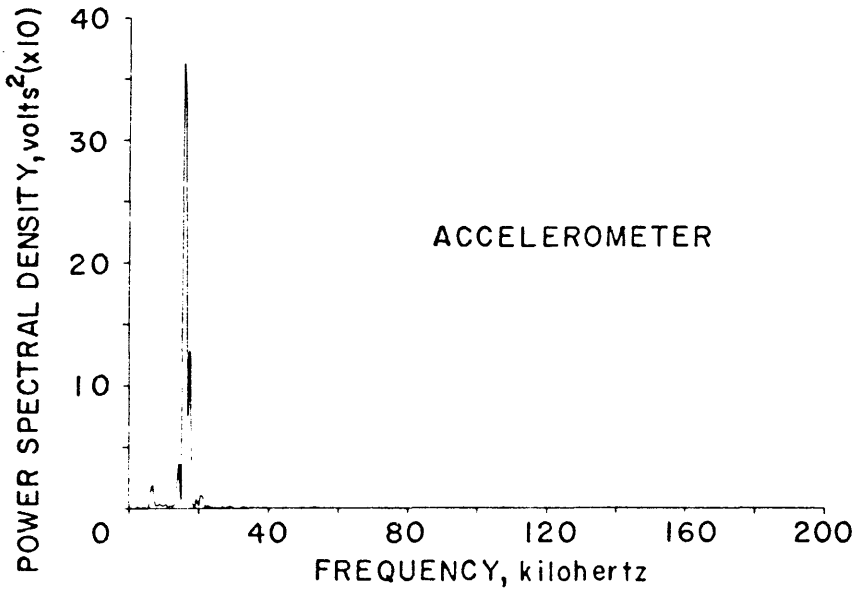

Figure 22: The amplitude spectrum of the accelerometer. Energy is sharply peaked at the accelerometer's resonant frequency of 16 kHz.

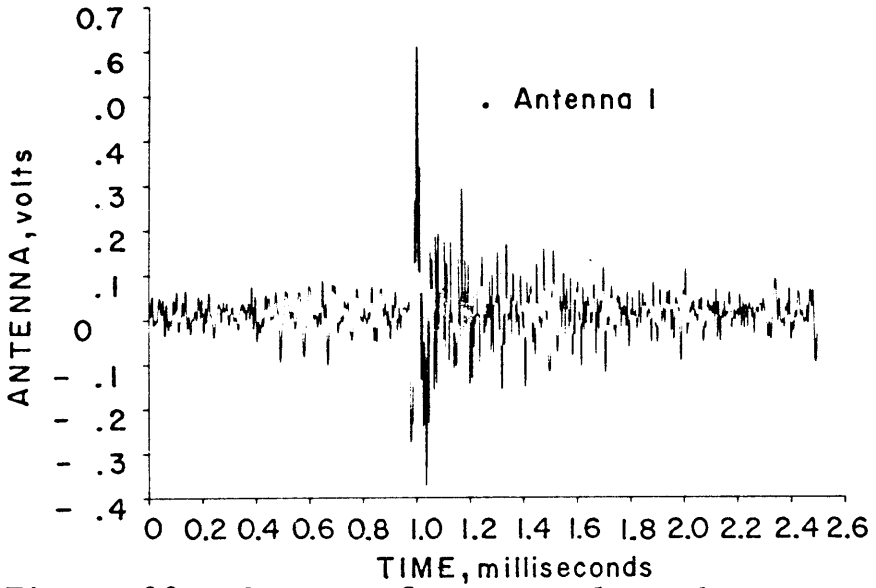

Figure 23: Output of antenna 1, Red Texas Granite sample #38. Response begins at .96 msec. and attains a maximum peak-to-peak amplitude of .99V.

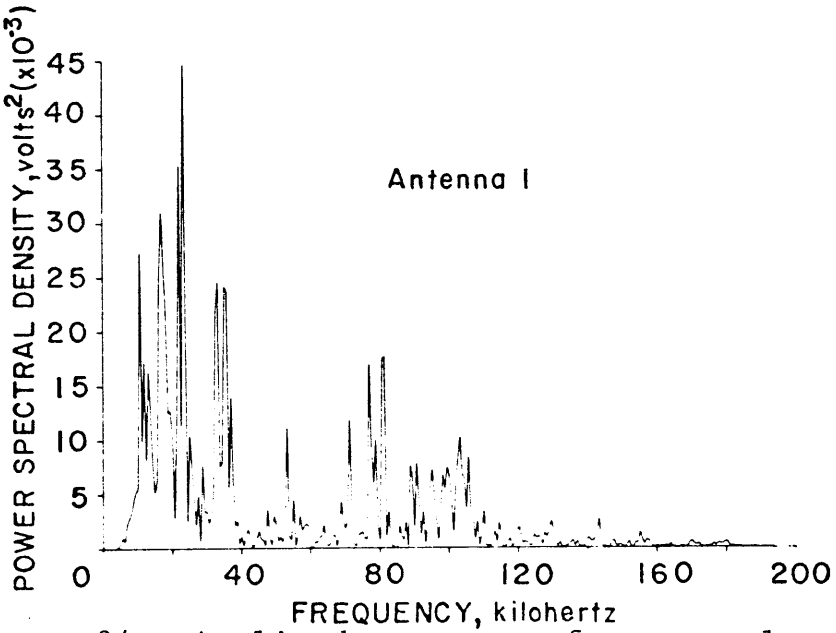

Figure 24: Amplitude spectra of antenna 1 output. The spectrum is more scattered than those for Galena Quartzite #47, but the majority of energy is still concentrated below 40 kHz. Major peaks occur at 10, 17, 22, 23, 33, and 35 kHz.

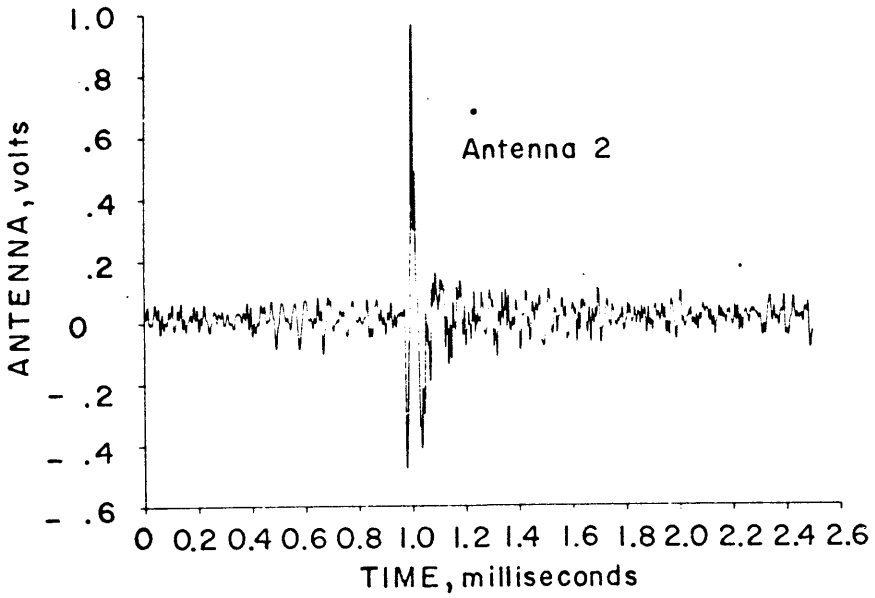

Figure 25: Response of antenna 2 to a preliminary fracture of Red Texas Granite. Maximum amplitude is 1.4V and response begins at .96 msec.

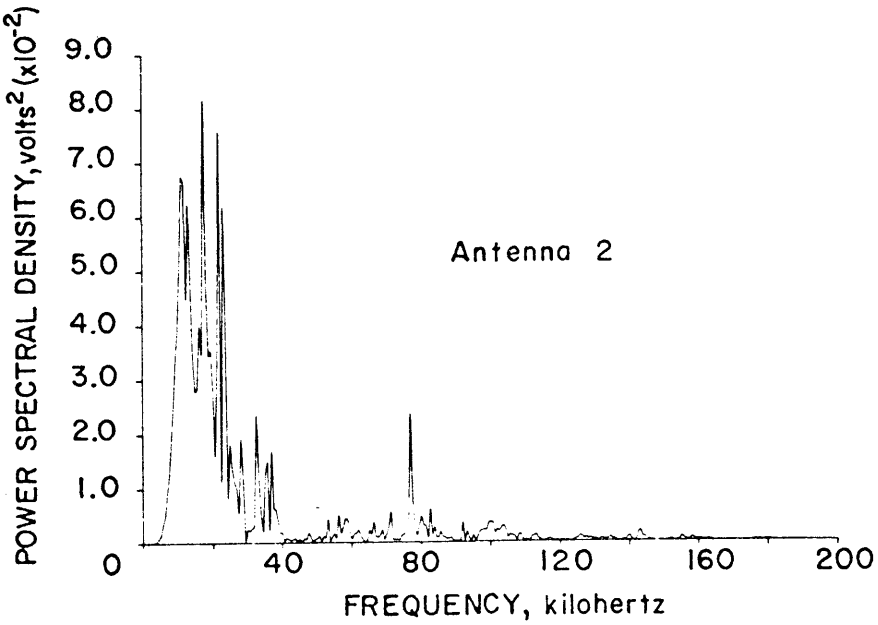

Figure 26: Spectrum of Figure 25. Energy lies almost exclusively below 40 kHz with major peaks at 11, 13.5, 17.5, 22, and 23 kHz.

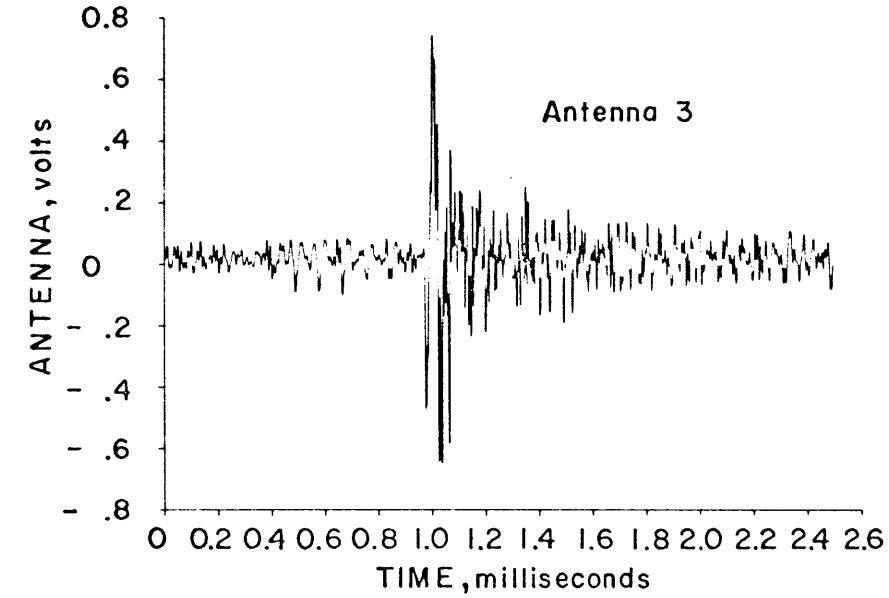

Figure 27: Antenna 3 output showing inception of impulsive event at 0.96 msec. Maximum peak-to-peak amplitude is approximately 1.4 V.

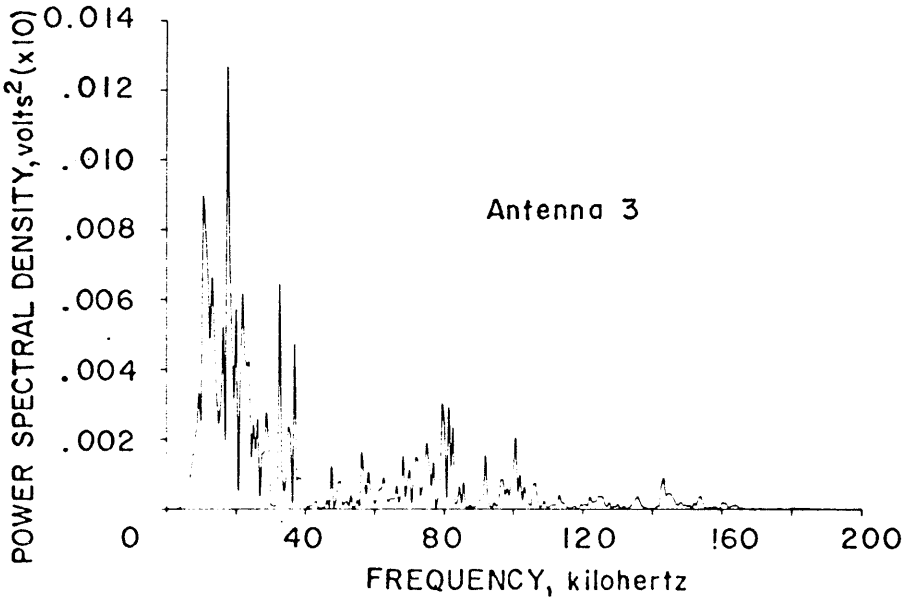

Figure 28: Spectrum of antenna 3, Red Texas Granite #38. Roughly the same behavior is observed as in Figures 24 and 26. Peaks in the spectra occur at 11, 18, and 33 kHz.

they should continue responding, following the wave forms of the other devices, which they do not. As with the Galena Quartzite, different antennas show different amplitude responses. While there are no moment changes available to infer the direction of crack growth, the antenna responses imply that the crack initiated in the upper half of the sample and grew in the +Y direction, or vice versa. Although slightly less peaked than the spectra of Galena Quartzite, antenna spectra for this event still peak below 40 kHz. Some of the frequency content in the power spectra is due to noise associated with the analog tape deck.

The final failure of this sample of Red Texas Granite involved a total load drop of 214 kN (Figure 29). Axial load shows a gradual decrease until about 1.4 msec where its slope suddenly decreases and catastrophic failure occurs. Figures 30, 31, and 32 are the three antenna responses. All three antennas are responding to radiated energy throughout this entire period, and bursts from them cannot be associated with appreciable single load drops before 1.4 msec. However, all show bursts before what is normally called "failure" on the load curve. This is especially true on antenna 3 (Figure 32) which overdrives and paralyzes its amplifier and filter system at 0.7 msec. Overdriving occurs on all antennas, but at different times and

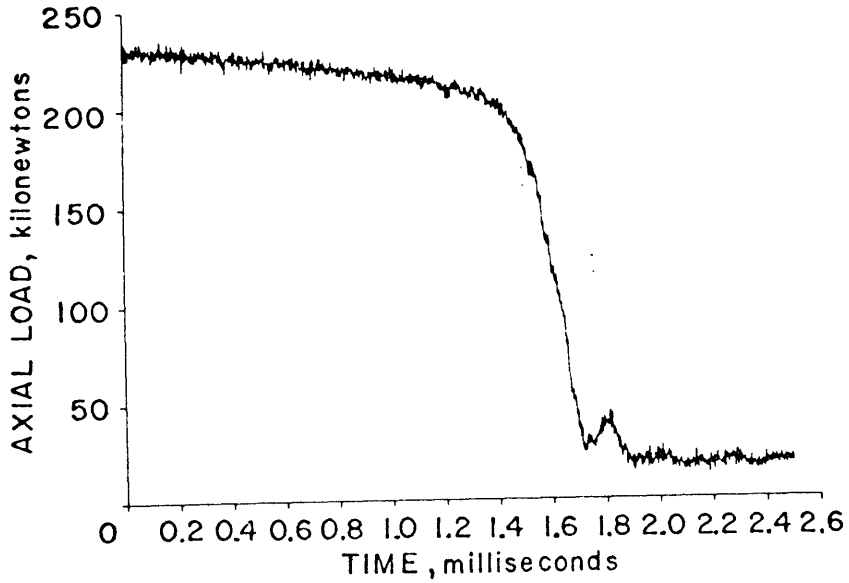

Figure 29: Axial load for Red Texas Granite #38 at final failure of the sample. Load decreases gradually until 1.4 msec where the slope radically decreases. This is the point of sample failure. Total load drop was about 214 kN.

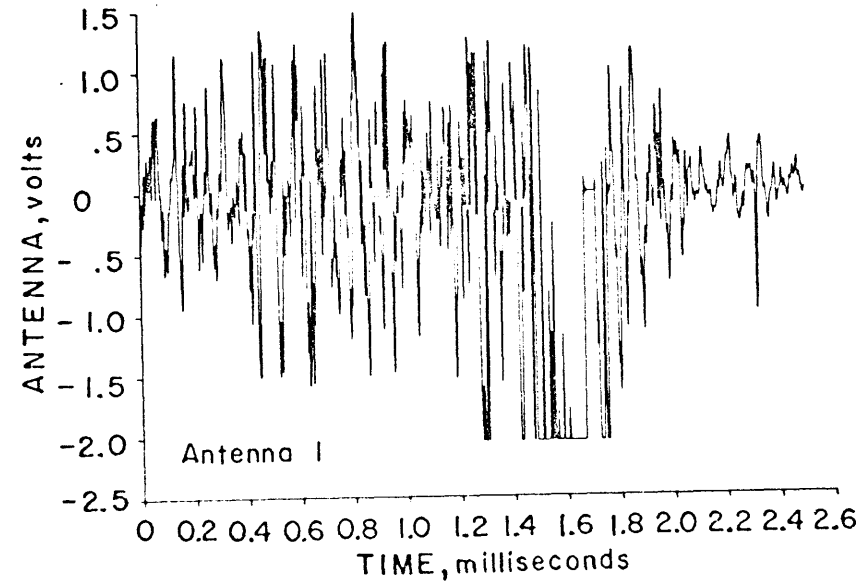

Figure 30: Antenna 1 response to the final failure of Red Texas Granite #38. Note that high amplitude antenna responses begin long before the 1.4 msec time of failure on the load curve.

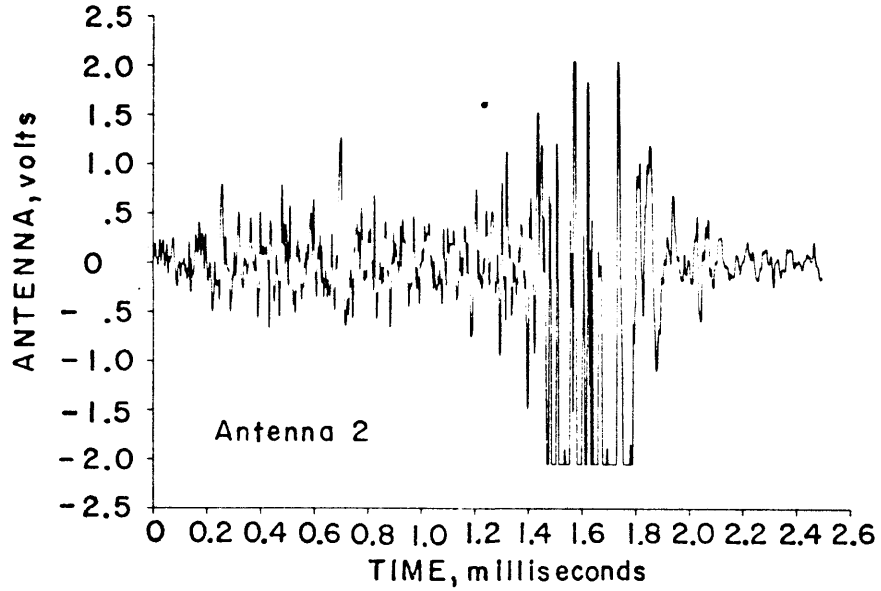

Figure 31: Response of antenna 2 to final failure of sample #38. Two major signals may be seen, the first at .7 msec. and the second at 1.4 msec. corresponding to final failure.

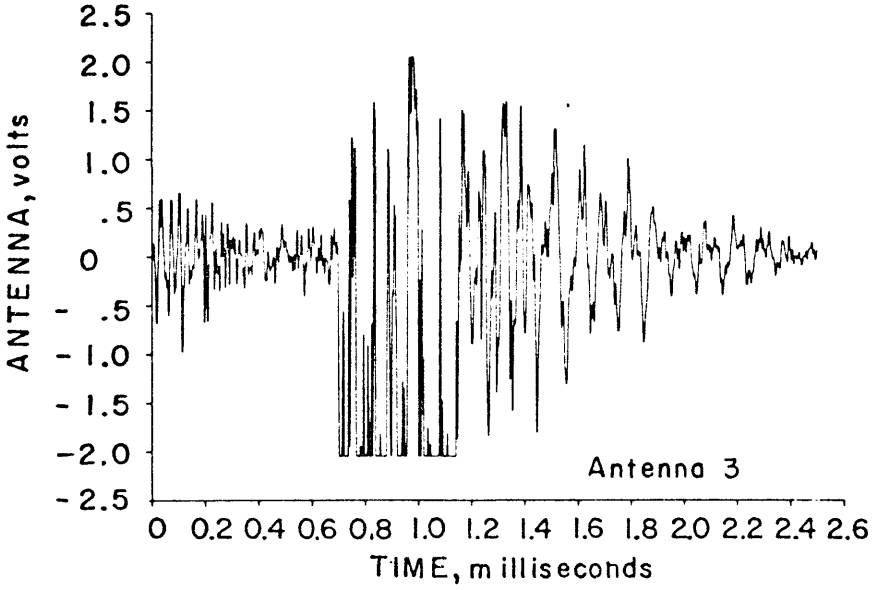

Figure 32: Antenna 3 signal excited by final failure of Red Texas Granite sample #38. Note how antenna becomes overdriven as early as .7 msec., long before final catastrophic failure.

this can be interpreted as another indication of directionality where the amplitude of emission is far greater in one direction than in others.

Results of this test show that small load drops long before final failure have associated EM bursts and that as the sample approaches failure, emission occurs even when there is only a gradual load drop and not sudden failures.

C. Barre Granite: Test #42

Barre Granite is a light colored, medium grained, biotite granite. It differs from Red Texas Granite in grain size and ultimate strength. Figure 33 shows the axial load at final failure for a Barre Granite sample. It shows a series of six distinct failure events separated by intervals of load stabilization. This contrasts with a smoother, more gradual load drop associated with the failure of the coarser grained Red Texas Granite. Very large antenna responses result from the failure of this specimen (Figures 34 to 36). All three antennas overdrove the system with the filters paralyzed after 1.8 msec. on antenna 1 and 1.3 msec. on antenna 3. The overdriving in all tests occurred because the EM emission was of a higher amplitude than expected. Again in this test, individual failure events on the load can be correlated with EM bursts and the amplitude of these bursts varies between antennas.

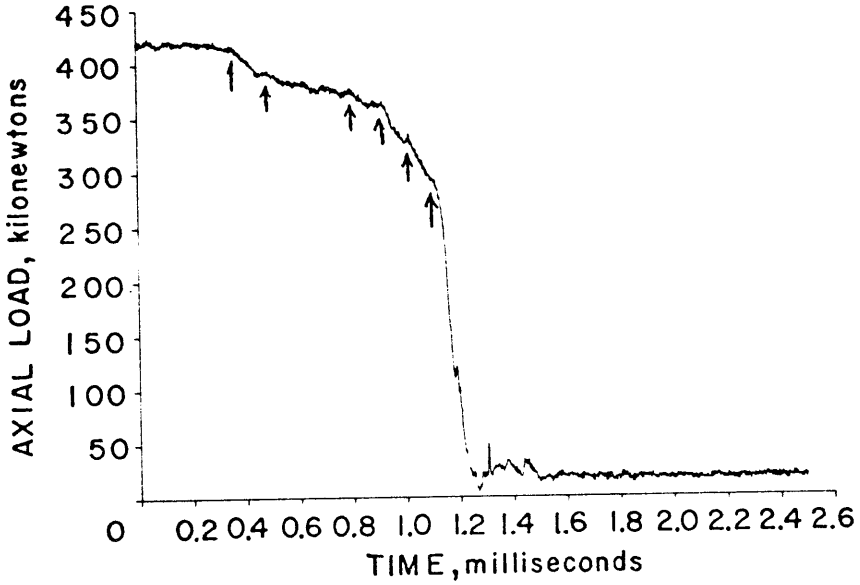

Figure 33: Axial load of Barre Granite sample #42 at final failure. For this sample five distinct failure events may be seen before final failure at 1.1 msec.

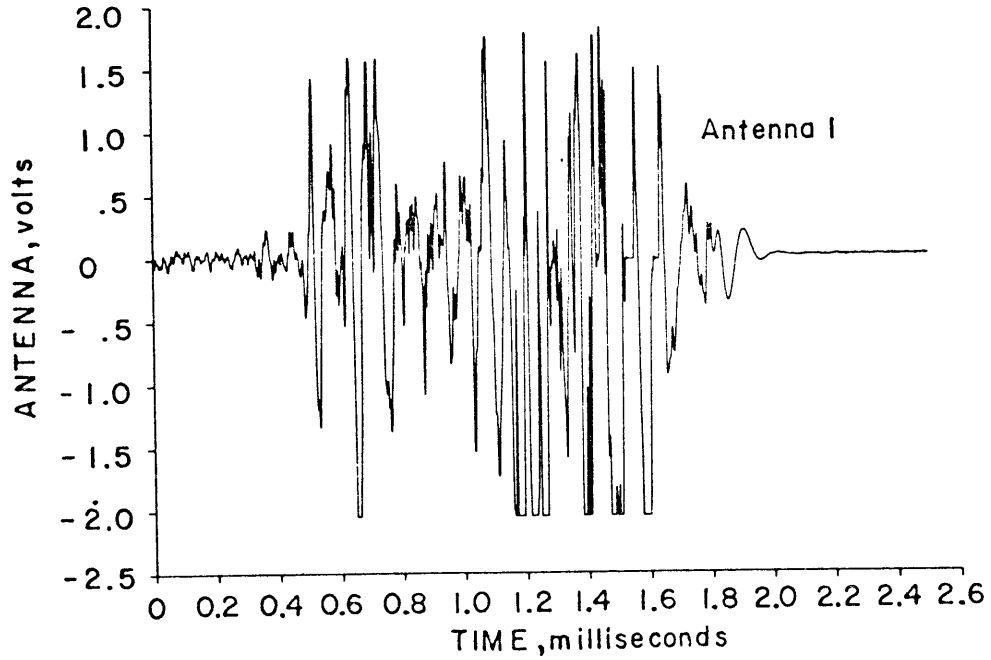

Figure 34: Response of antenna 1 to the failure of Barre Granite. Response begins with the first of the failures shown in Figure 33 and continue to form the complex waveform shown.

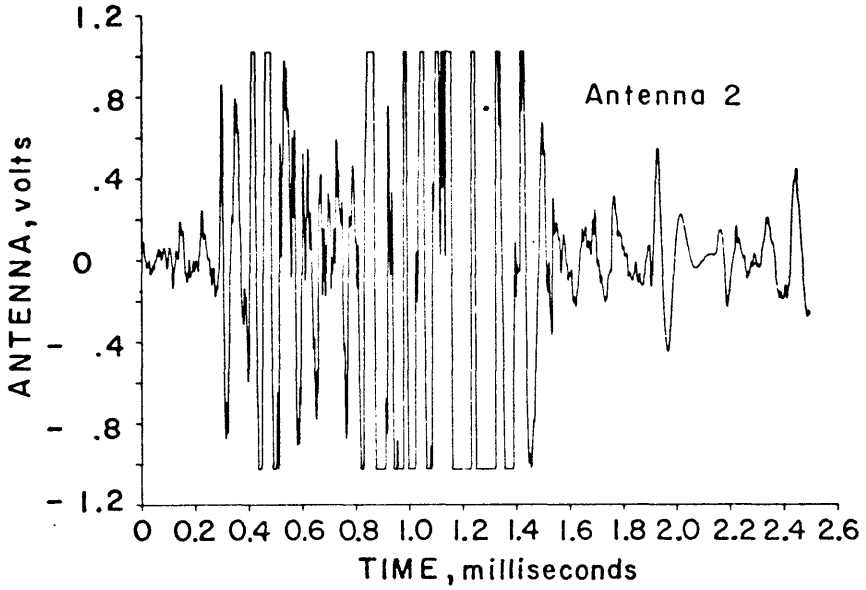

Figure 35: Antenna 2 output from Barre Granite Failure. Note that the amplitude scale of Figure 34 is twice that of Figure 35.

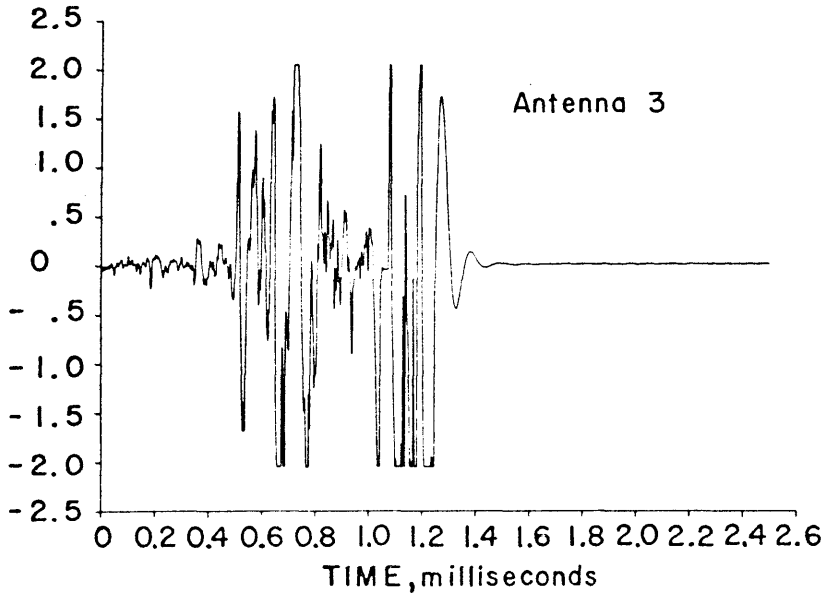

Figure 36: Output of antenna 3. After 1.4 msec. the amplifier and filter system of antenna 3 became overdriven and paralyzed.

D. Mather Iron Ore: Test #46

A powder X-ray diffraction analysis was performed on a sample of Mather Iron Ore by Dr. E. Booy of the Colorado School of Mines Geology department. From this it was learned that this fine-grained, rust colored taconite ore was composed mainly of quartz with minor amounts of magnetite, illite, kaolinite, and possibly a trace of hematite. This is a rock type different from those tested previously, but the behavior observed in Figures 37 to 43 is essentially the same. Brittle failure of the sample (as seen in the sudden load drop of Figure 37) is accompanied by violent changes in both moments (Figures 38 and 39), excitation of the AET (Figure 40), and short bursts of electromagnetic radiation (Figures 41 to 43). In this test, all three antennas had about the same amplitude response, although antenna 2 could possibly be slightly smaller.

E. Dakota Sandstone: Test #43

Dakota Sandstone is a fine to medium-grained, light colored sandstone with a quartz cement which will support an ultimate load of only 180 kN. This is a much lower strength material than those described earlier and it deforms nearly plastically. That is, there are really no large sudden load drops that could be associated with a distinct moment

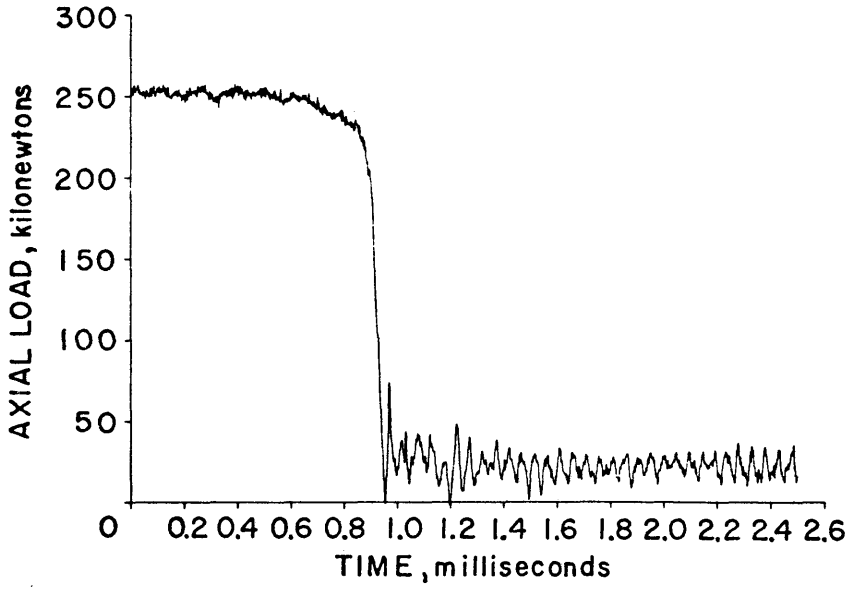

Figure 37: Axial load on Mather Iron Ore #46 at the point of its final failure. The very abrupt drop in load is indicative of a fine-grained, brittle material.

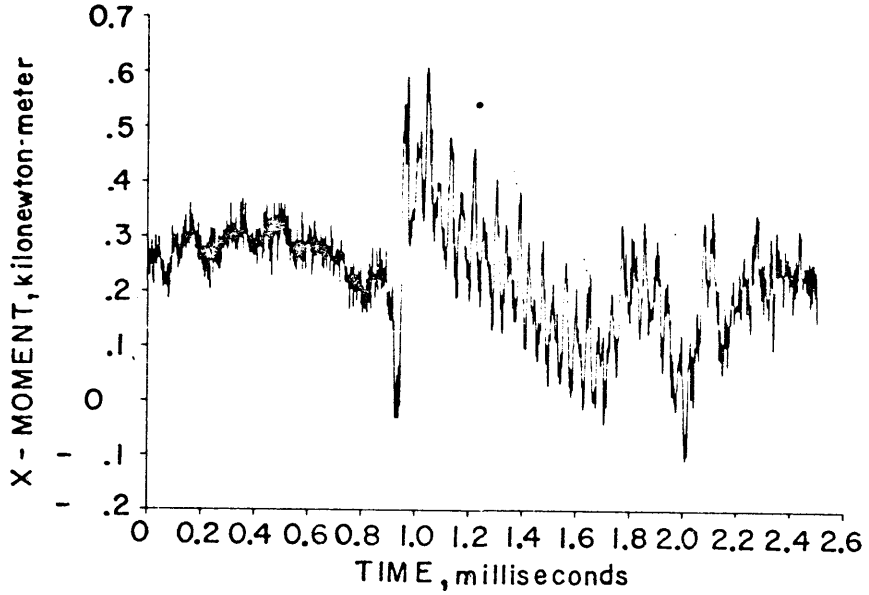

Figure 38: X component of the moment for the failure shown in Figure 37. Note the very violent reversals which occur as the sample fails.

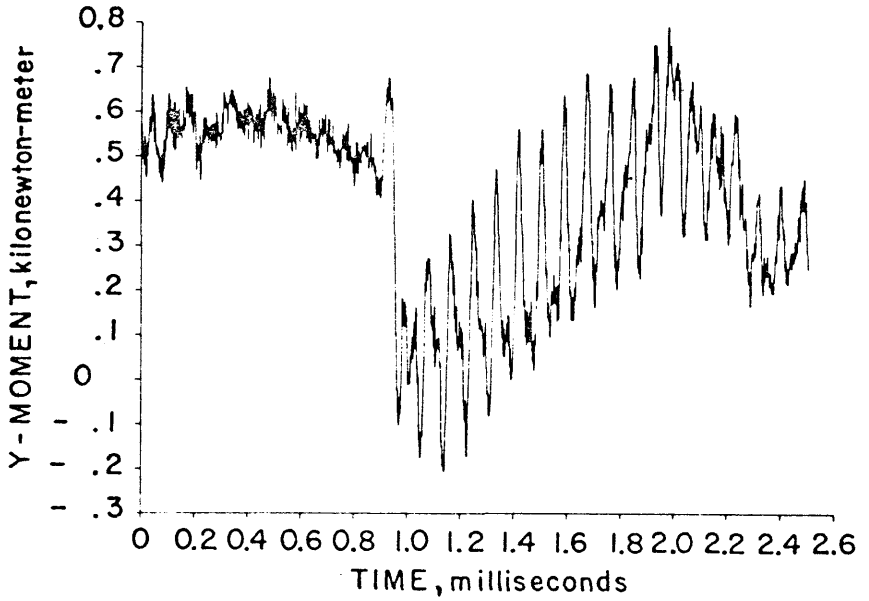

Figure 39: Y component of the moment for the failure of Mather Iron Ore sample #46. The rapid variations in moment correspond to inception of failure of the sample.

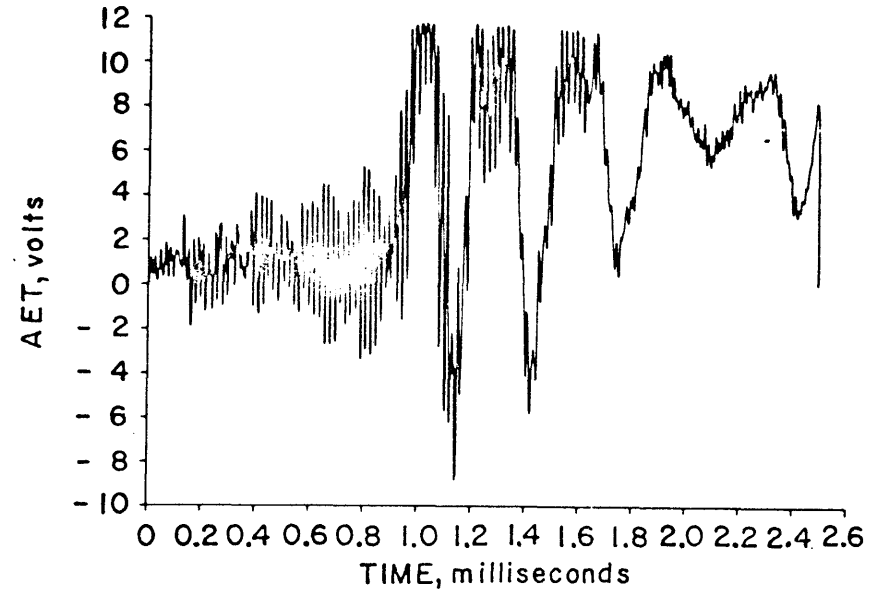

Figure 40: AET signal corresponding to the event shown in Figure 37. The AET begins responding as early as .1 msec. and continues ringing throughout the remainder of the trace.

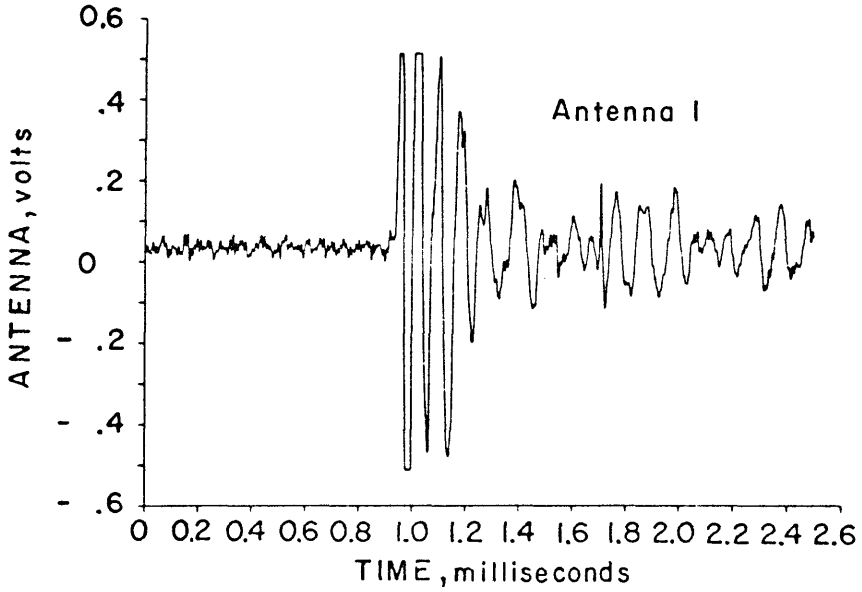

Figure 41: The impulsive response of antenna 1 to the failure of Mather Iron Ore #46. Inception of this event is slightly later in time than that indicated in Figures 37, 38, and 39, probably due to mislocation of the event within the sample.

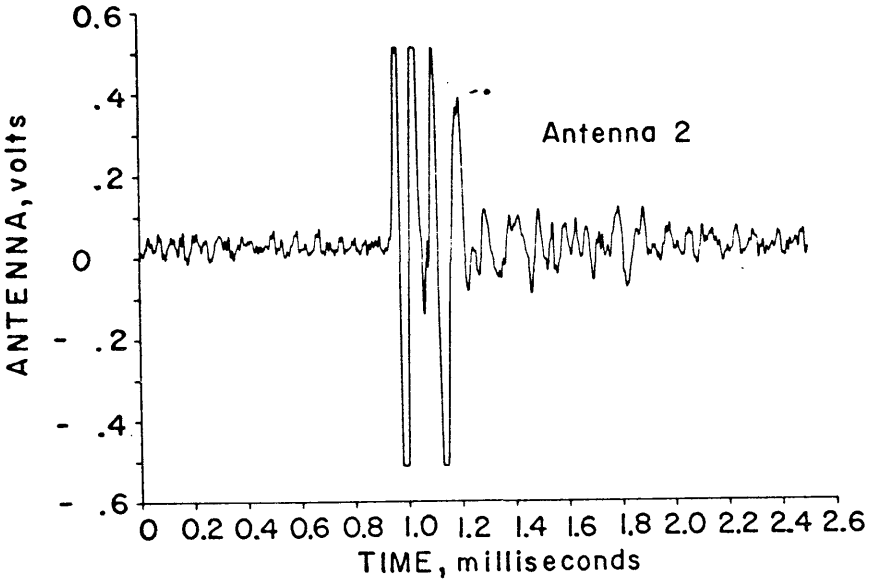

Figure 42: Antenna 2 response to final failure. Note both the shorter duration and lower amplitude of the signal than those seen for other rocks.

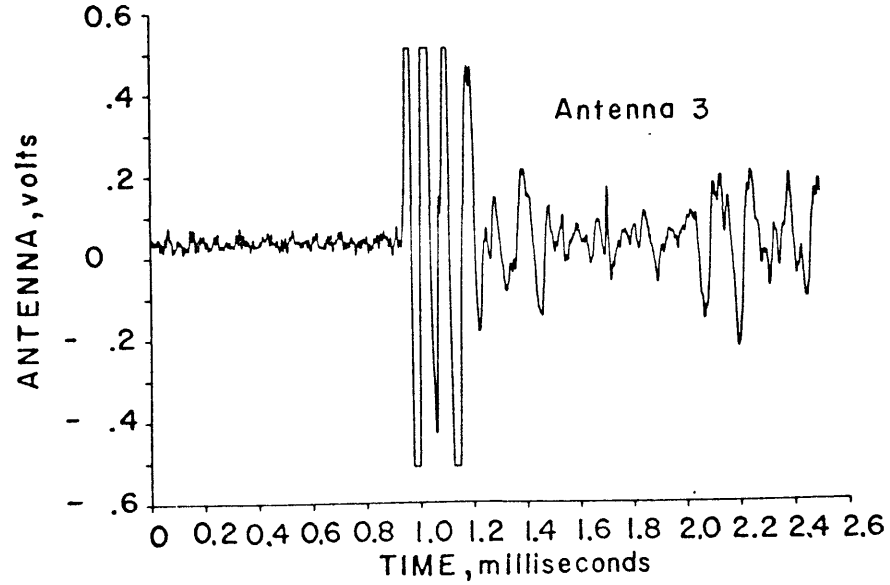

Figure 43: Antenna 3 signal at failure of sample #46.

of failure. Failure of this rock (and the Carthage Marble described next) seems to take place more by cataclastic granulation than by brittle fracture and its associated sudden load drops.

Although all other devices showed at least some indication of failure, none of the antennas showed any EM response above the ambient noise (Figure 45). This may be due to the more random orientation of the electrical axes of the quartz grains, or that no individual failure event released enough energy of itself to initiate a response from the antennas.

F. Carthage Marble: Test #44

This another relatively soft rock which does not have a sudden catastrophic failure, but rather undergoes a gradual cataclastic type of failure. Figure 46 is the most dramatic load drop associated with the final failure of the sample and the most abrupt drop here is 8 kN at 0.80 msec. Like Dakota Sandstone none of the antennas show any indication of an EM response while other devices (moment, accelerometer) indicate failure around 0.8 msec. This could be due to a simple lack of generation of any electromagnetic energy for this rock, or that the possibility for emission exists (correct rock composition) but stress drops of individual events were too gradual to generate the energy

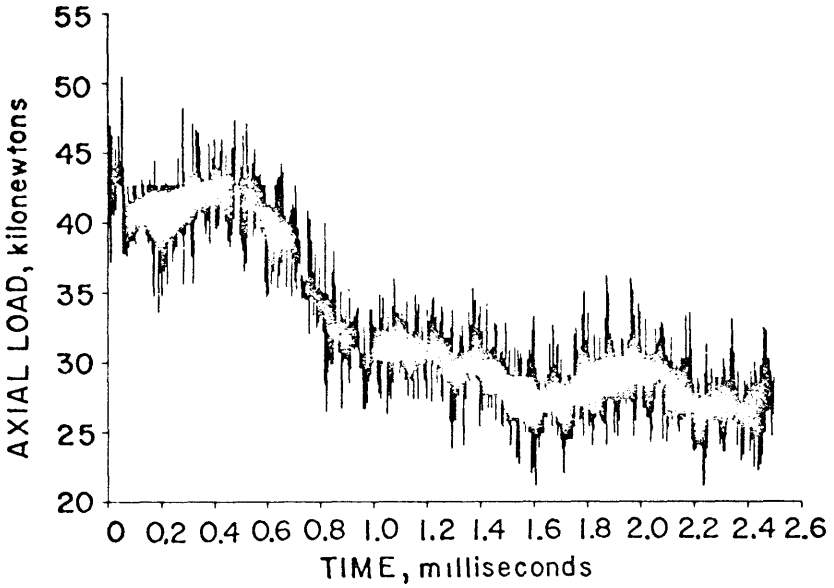

Figure 44: Largest single load drop associated with the failure of Dakota Sandstone sample #43. Load drop is approximately 14 kN.

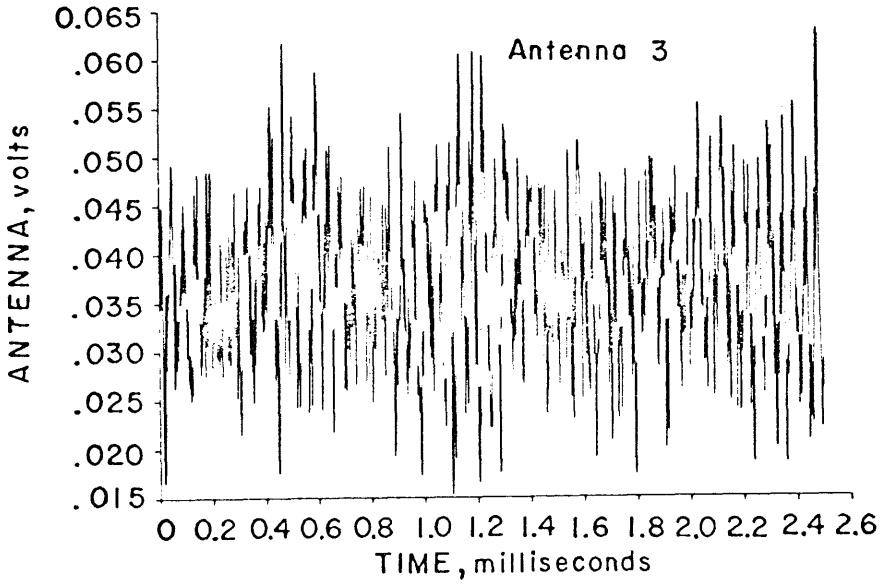

Figure 45: Response of antenna 3 to the failure event in Dakota Sandstone shown in Figure 44. No emission above the noise level is detectable.

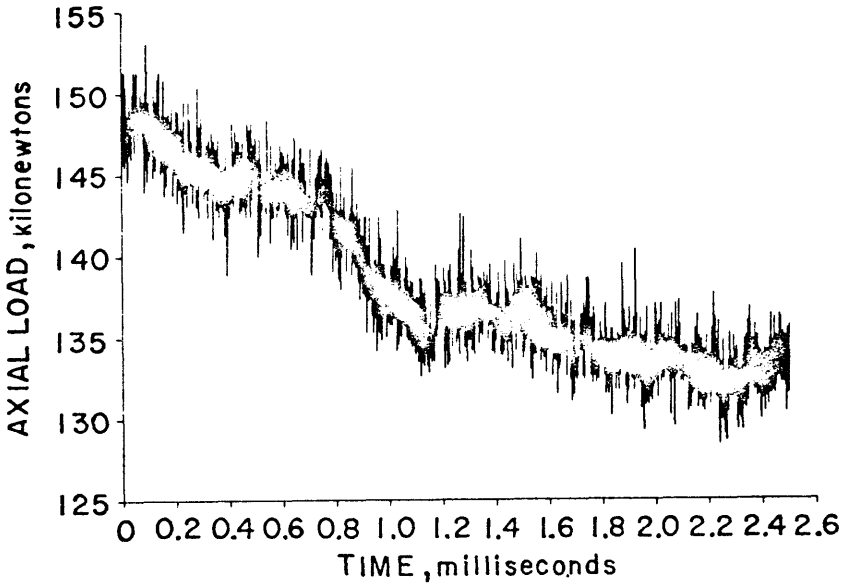

Figure 46: Axial load at failure of Carthage Marble #44. This sample, like Dakota Sandstone, has gradual, almost plastic, failure.

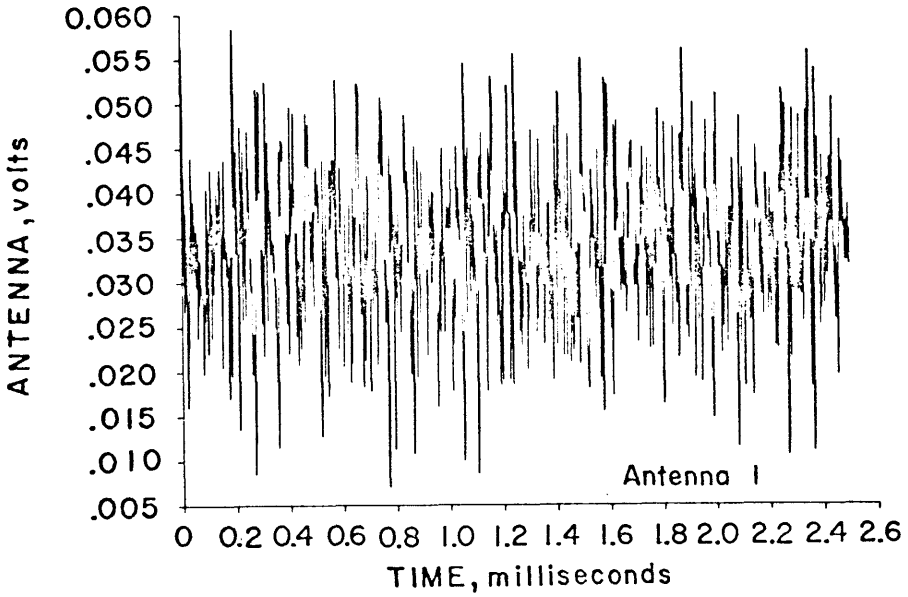

Figure 47: Antenna 1 response during the failure of Carthage Marble #44. Like Dakota Sandstone, there is no signal visible above the noise level.

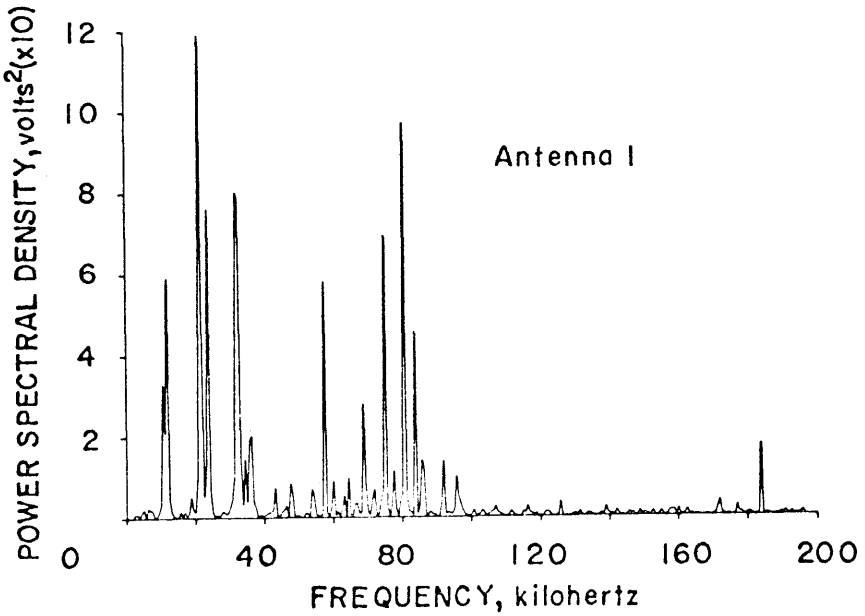

Figure 48: Amplitude spectra of the antenna signal of Figure 47. This spectra differs significantly from those of samples which emit. Instead of being peaked below 40 kHz, significant energy exists between 60 kHz and 90 kHz.

needed for radiation. The former explanation seems to be the more likely.

V. Discussion

A. Major Results

Analysis of the data collected reveals five major observations.

1) The formation of failure zones within certain rock materials is accompanied by bursts of electromagnetic radiation.

2) Where radiation is observed its energy is concentrated below 40 kHz and there is almost no energy between 40 kHz and 160 kHz, regardless of rock type or grain size.

3) Emission of this radiation seems to be directional, with the maximum radiation direction colinear with the direction of crack growth.

4) Emission was seen for all quartz-bearing rocks except sandstone. A non-piezoelectric marble was tested and gave no emission.

5) It was also observed, like Nitzan (14), that the amplitude of emission seemed to be independent of load, however it did not seem to be independent of load drop. Larger load drops for individual events is a measure of crack size and the energy released. It has been observed that as these load drops (or accelerometer responses) increase in amplitude, the amplitude of the EM radiation also increases.

Referencing the work of Nitzan, he observed emission in the range of 1 MHz to 10 MHz using a 40 db amplifier with a bandwidth of .1 to 400 MHz. In this frequency range he observed a nearly flat frequency response. In the work performed here, the frequency band was lowered to 10 kHz to 400 kHz and a much different spectral response was observed (Figures 11, 13, 15, 24, 26, and 28). The difference between the peaked emissions seen in this work and Nitzan's "white" spectrum may be explained in two ways. The first is that two peaks in emission occur, the first below 40 kHz and the second above 1 MHz. The second is that there is one major emission peak, below 40 kHz. Radiation most probably occurs over the entire spectrum but at a lower energy level than that seen between 10 kHz and 40 kHz. Nitzan did not see the low frequency peaks because his system was not tuned for it. The choice of investigating the lower frequency band seems to have been fortuitous.

The most important result of this work is the discovery of possible directionality or creation of nodal planes in the near or static electromagnetic field. This not only presents a possible method of mapping the direction of propagation of failures, but also gives insights into the mechanism of failure and what happens at the tip of a growing crack on a microscopic scale. The apparent directionality

indicates that the crack cannot be viewed as a simple isotropic radiator. There is some focusing mechanism active, be it simply the creation of interference patterns as with parasitic antenna arrays, or some other mechanism which creates "beams" of electromagnetic energy.

B. Emission Models

In his first work in 1977, Nitzan put forward the hypothesis that the rapid decay of the piezoelectric field with the stress drop accompanying fracture was the most probable mechanism of emission. He quoted figures for field gradients of 10^8 V/m at the failure point of quartz and charge displacements of 10^{-7} C for an effected volume of 1 cm^3. He proposed that the frequency of emission was related to the rate at which stress was released and so was inversely proportional to the grain size.

Experimental work done here supports some points of this hypothesis and creates problems for others. The presence of piezoelectric materials is definitely a criterion for RF emission, but just how emission is related to the creation of intense piezoelectric fields is still not completely understood. Rock types tested in this paper ranged from very coarse-grained Red Texas Granite to very fine-grained Galena Quartzite and Mather Iron Ore. In the lower frequency range examined, no significant variation in power spectra

with grain size can be observed. This seems to indicate that whatever mechanism is responsible for emission it is more dependent on the generation of intense fields than the size of the grains broken. It is possible that two different mechanisms are responsible for emission in the two different frequency bands investigated. Whatever mechanism is proposed for the generation of the RF signals, it must have the capability of producing a directional signal. Relative displacement of charges as a crack is formed could possibly accomplish this.

A slightly different mechanism involves the acceleration of exoelectrons freed by the formation of a failure zone (26,27,28). It has been reported that the piezoelectric field of a quartz crystal under local stress can reach values of 10^8 V/m (14). Any electron freed by failure will be accelerated by this field and will radiate energy as it is captured by nearby ions or otherwise decelerated (25). If the piezoelectric fields created in the stressed rock have a much greater gradient in one direction than in any other, confinement of these exoelectrons into a fairly narrow beam could occur, resulting in a directional radiation pattern (25). If the tip of the growing crack were to reach the surface with its high potential gradient, these exoelectrons could be ejected from the surface of the rock with consid-

erable energy. This fits with the observation of exoelectrons with as high an energy as 100 keV (27). In rocks which do not contain piezoelectric minerals, exoelectrons are still produced but there are no strong fields present to accelerate or confine them and so no RF radiation is observed.

Most of the signals associated with small load drops (small fractures) are of very short duration consisting of only a few cycles. Any electric field producing such a signal must therefore, also decay rapidly with a very high damping on its oscillation. If emission were due solely to the creation and rapid decay of electric fields with fracture, the damped oscillation of the crystal lattice and subsequent buildup and decay of fields should be observable. Unless this oscillation is very highly damped or of very low amplitude, its effect does not seem to be present. It is possible, however, that the first of the RF signal is due to one type of mechanism and the trailing edge to low amplitude ringing. Complex waveforms observed at failure could then be composed of the superposition of the different signals.

In addition, it has been observed (12) that the piezoelectric field for a rock aggregate will increase only up to a certain saturation level. The potential for a quartz-bearing material will only go to so great a value, no matter how many crystals are fractured at a time. This would

seem to limit the magnitude of radiation caused by rapid field decay. If, on the other hand, emission derives a significant amount of its energy from the acceleration of charged particles, the more electrons freed, even assuming a constant accelerating E-field, the more energy available for radiation. Hence, larger failure zones should generate larger EM signals. This fracture size-radiation amplitude relationship has been observed experimentally and so gives weight to the hypothesis that some sort of mechanism of this nature is in effect.

Additional minor sources of energy may also contribute to the RF emission. These include the creation of transient electron-inertia pulses (15,16,17), radiation from hot rock particles, and possibly high frequency streaming potentials. The creation of electron-inertia pulses was described in part II and is probably of minor importance due to the lack of free conduction electrons in normal rock materials. Temperature in excess of 200° C have been recorded at the tip of growing cracks (Brady, personal communication, 1979). This energy must be radiated and if the failure zone could be idealized as a black body radiator, this is possibly an additional energy source. Streaming potentials are created in rocks which are saturated with a conducting fluid. The creation of micelles along pore walls and the

differential motion of the interstitial fluid and charged pore rock creates a potential which can be quite substantial. A high frequency elastic pulse propagating through an area close to the failure zones which is saturated should give rise to this sort of potential. Scholtz (2) reported a frequency content of 100 kHz to 1 MHz for microfracturing of rock materials indicating that frequencies high enough to get into the RF range do exist. This, however, does not explain emission seen in this experiment as all samples had been stored in air for at least two years and so were thoroughly dry. Thus the presence of water in the region of the failure zone is not a necessary condition for the emission of RF radiation. In actual earth conditions the streaming potential could present a sizable addition to RF radiation.

It should be stressed that none of the above mechanisms can be ruled out, nor can one be overwhelmingly favored over all others. It is very possible that all exist and contribute to some portion of the EM radiation observed. Laboratory work has not progressed far enough to select one model to the exclusion of all others.

Finally, it seems rather coincidental that sferics reported to have accompanied earthquakes (18) should have frequencies of 10 kHz to 20 kHz, nearly the same frequencies

as the major portion of the electromagnetic energy observed to be emitted from rock failure in this study. From this it seems possible that these sferics are the product of the larger scale failure of rocks during earthquakes.

C. Applications

The most important application of this phenomenon is the monitoring of unstable rock faces in mines or possibly monitoring activity along faults. In mining applications an extremely portable system could be devised since the antenna need not be coupled directly to the rock face as with conventional geophones. An increase in the number or amplitude of events could signal an impending rock burst.

This system seems practical on a mine scale for two reasons. First, if, as is impled in this study, the amplitude of emission increases with crack size, mine type failures could produce significant signals. Secondly, calculations of skin depth for dry rock indicate a depth of penetration of the signal which is practical for mine scale operations. Assuming a resistivity of 10^5 ohm-m for dry granite, at 20 kHz the skin depth is on the order of 1000 m. Saturating fluids will reduce this value but to what extent is unknown.

VI. Conclusions

The fracture and failure of rock materials containing piezoelectric minerals has been shown to be accompanied by the emission of bursts of radio frequency electromagnetic energy. Detection of these bursts is a fairly simple operation requiring only an electrically short dipole antenna, and filters and amplifiers appropriate to the frequency band to be investigated.

Existence of these RF signals in the range of 10 kHz to 400 kHz has been observed, which, with Nitzan's (14) results, extends the known frequency range of emission to 10 kHz to 10 MHz, although it is very possible emission extends into lower and higher frequencies. Power spectra of antenna signals show the energy to be sharply peaked between 10 kHz and 40 kHz. This spectral peak corresponds well with the 10 kHz to 20 kHz sferics reported by Derr (18) to accompany some earthquakes.

The RF emission observed had two other characteristics. It increases in amplitude with increasing crack size, and it exhibits a degree of directionality. As the amplitude of acceleration and acoustic emission increases, so does the amplitude of RF emission. An array of three dipole antennas placed around the sample tested showed amplitude variations for the same event of as much as 4:1, which indicates a

fairly high degree of directionality in emission. The maximum direction of radiation appears to be colinear with the direction of propagation of the crack.

While emission is seen only for rocks containing piezoelectric minerals, just what the relation between piezoelectric fields and emission is, is not fully understood. Proposed mechanisms of emission include the rapid drop in piezoelectric field with fracture of the crystal and/or the acceleration of freed exoelectrons by the very intense local piezoelectric field gradients.

The application of EM radiation to monitor slope and rock wall instabilities appears promising as larger events cause larger signals and in the 20 kHz range dry rock is fairly transparent. On a still larger scale, depending on rock and failure type, it may become feasible to monitor fault traces for both activity and rupture propagation direction by using arrays of antennas.

VII. Appendix A: Sample Type and Size

Sample No.	Rock Type	Length	Diameter	Tolerance
1	RTG	13.50	——	.0005
2	RTG	13.50	——	.0005
3	RTG	13.50	——	.0008
4	PPG	13.26	5.35	—
5	PPG	13.50	——	.0003
6	PPG	13.48	——	.002
7	PPG	13.48	——	.001
8	BG	13.49	5.35	.0015
9	BG	13.48	5.34	.0018
10	RTG	13.50	——	.0008
11	RTG	13.50	——	.0008
12	RTG	13.50	——	.001
13	RTG	13.50	——	.002
14	RTG	13.50	——	.001
15	RTG	13.50	——	.001
16	RTG	13.50	——	.0005
17	RTG	13.50	——	.0005
18	RTG	13.50	——	.0008
19	RTG	13.50	——	.0005
20	RTG	13.50	——	.0008
21	RTG	13.50	——	.0005
22	RTG	13.50	——	.001
23	RTG	13.50	——	.001
24	RTG	13.50	——	.0008
25	RTG	13.50	——	.001
26	RTG	13.50	5.40	—
27	RTG	13.50	5.40	—
28	RTG	13.50	5.40	—
29	RTG	13.50	5.40	—
30	CM	12.70	——	.0008
31	DSS	13.47	——	.0008
32	BG	13.50	5.34	.002
33	RTG	13.50	5.40	—
34	RTG	13.50	5.40	—
35	RTG	13.50	5.40	—
36	RTG	——	——	—
37	BG	——	——	—
38	RTG	13.50	5.40	—
39	RTG	13.50	5.40	—
40	BG	13.50	5.35	—
41	BG	13.45	5.35	—
42	BG	13.47	5.35	—

Sample No.	Rock Type	Length	Diameter	Tolerance
43	DSS	13.50	——	.001
44	CM	12.70	——	.002
45	MIO	9.53	3.85	—
46	MIO	9.53	3.85	—
47	GQ	13.50	5.47	—

RTG - Red Texas Granite
BG - Barre Granite
PPG - Pikes Peak Granite
DSS - Dakota Sandstone
CM - Carthage Marble
MIO - Mather Iron Ore
GQ - Galena Quartzite

All lengths, tolerances, and diameters are given in centimeters.

VIII. Appendix B: Computation of Travel Time Shifts

Since electromagnetic waves travel at the speed of light and other signals travel to monitoring devices at the velocity of sound in rock, a time shift between the two exists. This shift causes all other devices to appear shifted later in time than the antennas. If an exact location of the event within the sample were available, the time required for the information to travel to the detection devices could be computed and subtracted from plots. This would then theoretically bring the plots into time coincidence since all devices would be referenced to the antennas because the EM waves effectively arrive instantaneously.

An exact location of events within the sample was not available so an average travel path in the rock of 6.3 cm (4.8 cm for the iron ore) was assumed. Computation of the time to be removed from devices other than the antennas proceeded as follows:

- average distance in rock $\simeq$ 6.3 cm
- average distance in iron ore $\simeq$ 4.8 cm
- maximum distance in steel to accelerometer and AET $\simeq$ 33.0 cm
- average distance in steel to load and moment gauges $\simeq$ 10.2 cm

- velocity of sound in steel ≃ 5486 m/sec.
- velocity of sound in granite ≃ 3810 m/sec.
- velocity of sound in iron ore ≃ 5273 m/sec.
- velocity of sound in marble ≃ 5060 m/sec.
-velocity of sound in sandstone ≃ 2438 m/sec.
- velocity of sound in quartzite ≃ 5334 m/sec.

- maximum travel time in steel ≃ 60 μsec.
≃67 μsec (iron ore tests)

- average time in:
  - granite ≃ 17 μsec
  - iron ore ≃ 9 μsec
  - marble ≃ 12 μsec
  - sandstone ≃ 26 μsec
  - quartzite ≃ 12 μsec

- travel time in steel to load and moment gauges ≃ 18.5 μsec.

To get a complete time shift, the shift due to head skew between channel 3 and other channels must be added to the delay due to travel path. These skews are:

Channels	Skew Time (μsec)
3-1	.26
3-5	.07
3-7	.42
3-8	2.79
3-9	.32
3-10	2.20
3-12	2.56
3-14	2.10

So the final time shift for the different samples and channels are (in μsec.)

Channel	Granite	Iron Ore	Quartzite, Marble	Sandstone
3-1	.26	.26	.26	.26
3-5	.07	.07	.07	.07
3-7	77.4	76.4	72.4	86.4
3-8	79.8	78.8	74.8	88.8
3-9	17.3	9.3	12.3	26.3
3-10	37.7	29.7	32.7	46.7
3-12	38.1	30.1	33.1	47.1
3-14	37.6	29.6	32.6	46.6

Channel	Device
1	Antenna 1
3	Antenna 2
5	Antenna 3
7	AET
8	Accelerometer
9	PPT
10	Axial Load
12	Moment: X Component
14	Moment: Y Component

The times for channel 9 (PPT) are less than those for other devices (except antennas) because it was placed directly on the rock and was assumed to have an average travel path of 6.3 cm in the rock for all samples.

Table 1

Phase and Time Shifts Between
Channels on the Sangamo Sabre X Tape Deck

Channels	Phase Shift (degrees)	Time Shift (μsec)
1-3	- 18.9	- 1.05
1-5	- 13.1	- .73
1-7	+ 9.5	.53
1-9	+ 11.0	.61
1-11	+ 47.6	2.64
1-13	+ 88.0	4.89
3-5	+ 5.1	.28
3-7	+ 30.0	1.67
3-9	+ 23.3	1.29
3-11	+ 72.9	4.05
3-13	+103.7	5.76
2-4	+ 17.5	.97
2-6	+ 25.0	1.39
2-8	+ 41.0	2.28
2-10	+ 27.0	1.50
2-12	+ 13.1	.73
2-14	- 3.2	- .18
4-6	+ 7.8	.43
4-8	+ 25.0	1.39
4-10	+ 10.4	.58
4-12	- 2.3	- .13
4-14	- 23.3	- 1.29
1-2	+163.9	9.11
1-4	+189.1	10.51
1-6	+198.7	11.04
1-8	+220.0	12.22
1-10	176.9	9.83
1-12	202.8	11.27
1-14	170.1	9.45
2-3	-170.6	- 9.48
2-5	-173.2	- 9.62
2-7	-151.0	- 8.39
2-9	-154.6	- 8.59
2-11	-105.5	- 5.86
2-13	- 78.7	- 4.37

IX. Bibliography

1. Jaeger, J. C., Elasticity, Fracture, and Flow, New York, John Wiley & Sons, Inc., (1956).
2. Scholtz, C. H., Experimental Study of the Fracturing Process in Brittle Rock, Journal of Geophysical Research, 73, 1447-1454, (1968).
3. Booker, J. R., Dilatancy and Crustal Uplift, Pure and Applied Geophysics, 113, 119-125, (1975).
4. Rikitake, T., Dilatancy Model and Emperical Formulas for an Earthquake Area, Pure and Applied Geophysics, 113, 141-147, (1975).
5. Mjachkin, V. I., W. F. Brace, G. A. Sobolev, and J. H. Dieterich, Two Models of Earthquake Forerunners, Pure and Applied Geophysics, 113, 169-181, (1975).
6. Cherry, J. T., R. N. Schock, and J. A. Sweet, A Theoretical Model of the Dilatant Behavior of a Brittle Rock, Pure and Applied Geophysics, 113, 183-196, (1975).
7. Nur, A., A Note on the Constitutive Law for Dilatancy, Pure and Applied Geophysics, 113, 197-206, (1975).
8. Brady, B. T., Theory of Earthquakes, Part I: A Scale-Independent Theory of Rock Failure, Pure and Applied Geophysics, 112, 701-725, (1974).
9. Brady, B. T., Theory of Earthquakes, Part II: Inclusion Theory of Crustal Earthquakes, Pure and Applied Geophysics, 113, 149-168, (1975).
10. Brady, B. T., Theory of Earthquakes, Part III: Inclusion Collapse Theory of Deep Earthquakes, Pure and Applied Geophysics, 114, 119-139, (1976).
11. Brady, B. T., Theory of Earthquakes, Part IV: General Implications for Earthquake Prediction, Pure and Applied Geophysics, 114, 1031-1082, (1976).
12. Parkhomenko, E. I., Electrification Phenomena in Rocks, New York, Plenum Press, (1971).
13. Vorobev, A. A., V. M. Chasov, and V. F. Gordeev, Pulsed RF Radiation Produced by Scratching Some Dielectrics, Soviet Phys. Journal, 10, 126-128, (1977).
14. Nitzan, U., Electromagnetic Emission Accompanying Fracture of Quartz-Bearing Rocks, Geophysical Research Letters, 4, 333-336, (1977).
15. Kennedy, J. D., and C. W. Curtis, Transient Electron-Inertia Fields Produced by a Strain Pulse, The Journal of the Acoustical Society of America, 41, 328-335, (1967).
16. Moon, F. C., The Generation of Electromagnetic Radiation by Elastic Waves, Developments in Mechanics, 6, Proceedings of the 12th Midwestern Mechanics Conference, 623-630.

17. Moon, F. C., and S. Chattopadhyay, Magnetically Induced Stress Waves in a Conducting Solid-Theory and Experiment, Transactions of the AIME Journal of Applied Mechanics, 641-646, (1974).
18. Derr, J. S., Earthquake Lights: A Review of Observations and Present Theories, Bulletin of the Seismological Society of America, 63, 2177-2187, (1973).
19. Cohen, J., and S. Edelman, Piezoelectric Effect in Oriented Polyvinylchloride and Polyvinylfluoride, Journal of Applied Physics, 42, 3072-3074, (1974).
20. Edelman, S., Piezoelectric Polymer Stress Gauges, presented at Instrumentation for Civil Engineering Applications, Air Force Weapons Laboratory, Kirtland AFB, New Mexico, May 9, 1973.
21. Brady, B. T., G. A. Rowell, and L.P. Yoder, Physical Precursors of Rock Failure, submitted to Int. Journal of Rock Mechanics, (1980).
22. Terman, F. E., Radio Engineering, New York, McGraw-Hill Book Co., Inc., (1947).
23. Jasik, H., Radio Engineering Handbook, New York, McGraw-Hill Book Co., Inc., (1961).
24. Westman, H. P., Reference Data for Radio Engineers, New York, ITT Co., (1956).
25. King, R. W. P., and C. W. Harrison, Jr., Antennas and Waves: A Modern Approach, Cambridge, Mass., MIT Press, (1969).
26. Hoenig, S. A., Monitoring Failure Processes in Ceramic Materials by Means of Exoelectron Emission, NSF report, number unknown, (1974).
27. Hoenig, S. A., Monitoring the Ball-Milling Process by Means of Exoelectron Emission, Mining Congress Journal, 58, 34-35, (1972).
28. Good, R. H., and T. J. Nelson, Classical Theory of Electric and Magnetic Fields, New York, Academic Press, (1971).
29. Keller, G. V., and F. C. Frischnecht, Electrical Methods in Geophysical Propescting, New York, Pergamon Press, (1966).